75N11893

NASA TECHNICAL NOTE

NASA TN D-7753

NASA TN D-7753

EFFECTS OF LEADING-EDGE SWEEP ANGLE AND DESIGN LIFT COEFFICIENT ON PERFORMANCE OF A MODIFIED ARROW WING AT A DESIGN MACH NUMBER OF 2.6

by Robert J. Mack

Langley Research Center
Hampton, Va. 23665

RECEIVED
JAN 2 - 1975

NATIONAL AERONAUTICS AND SPACE ADMINISTRATION • WASHINGTON, D. C. • DECEMBER 1974

1. Report No. NASA TN D-7753	2. Government Accession No.	3. Recipient's Catalog No.
4. Title and Subtitle EFFECTS OF LEADING-EDGE SWEEP ANGLE AND DESIGN LIFT COEFFICIENT ON PERFORMANCE OF A MODIFIED ARROW WING AT A DESIGN MACH NUMBER OF 2.6		5. Report Date December 1974 6. Performing Organization Code
7. Author(s) Robert J. Mack		8. Performing Organization Report No. L-9446 10. Work Unit No. 760-65-11-02
9. Performing Organization Name and Address NASA Langley Research Center Hampton, Va. 23665		11. Contract or Grant No. 13. Type of Report and Period Covered Technical Note
12. Sponsoring Agency Name and Address National Aeronautics and Space Administration Washington, D.C. 20546		14. Sponsoring Agency Code

15. Supplementary Notes

16. Abstract

Nine wing models were tested in the high-speed section of the Langley Unitary Plan wind tunnel to study the effects of the leading-edge sweep angle and the design lift coefficient on aerodynamic performance and efficiency. The models had leading-edge sweep angles of 69.44°, 72.65°, and 75.96° which correspond to values of the design Mach-number—sweep-angle parameter $(\beta \cot \Lambda)_{DES}$ of 0.6, 0.75, and 0.9, respectively. For each sweep angle, camber surfaces having design lift coefficients of 0, 0.08, and 0.12 at a design Mach number of 2.6 were generated. The wind-tunnel tests were conducted at Mach numbers of 2.3, 2.6, and 2.96 with a stagnation temperature of 338.7 K (150° F) and a Reynolds number per meter of 9.843×10^6.

The results of the tests showed that only a moderate sweeping of the wing leading edge aft of the Mach line along with a small-to-moderate amount of camber and twist was needed to significantly improve the zero-lift (flat camber surface) wing performance and efficiency.

17. Key Words (Suggested by Author(s))
Aerodynamics
Wind-tunnel models
Supersonic speeds

18. Distribution Statement
Unclassified – Unlimited
STAR Category 01

19. Security Classif. (of this report)	20. Security Classif. (of this page)	21. No. of Pages	22. Price*
Unclassified	Unclassified	49	$3.75

*For sale by the National Technical Information Service, Springfield, Virginia 22151

EFFECTS OF LEADING-EDGE SWEEP ANGLE AND DESIGN LIFT COEFFICIENT ON PERFORMANCE OF A MODIFIED ARROW WING AT A DESIGN MACH NUMBER OF 2.6

By Robert J. Mack
Langley Research Center

SUMMARY

Nine wing models were tested in the high-speed section of the Langley Unitary Plan wind tunnel to study the effects of the leading-edge sweep angle and the design lift coefficient on aerodynamic performance and efficiency. The models had leading-edge sweep angles of 69.44°, 72.65°, and 75.96° which correspond to values of the design Mach-number—sweep-angle parameter $(\beta \cot \Lambda)_{DES}$ of 0.6, 0.75, and 0.9, respectively. For each sweep angle, camber surfaces having design lift coefficients of 0, 0.08, and 0.12 at a design Mach number of 2.6 were generated. The wind-tunnel tests were conducted at Mach numbers of 2.3, 2.6, and 2.96 with a stagnation temperature of 338.7 K (150° F) and a Reynolds number per meter of 9.843×10^6.

The results of the tests showed that only a moderate sweeping of the wing leading edge aft of the Mach line along with a small-to-moderate amount of camber and twist was needed to significantly improve the zero-lift (flat camber surface) wing performance and efficiency. Maximum lift-drag ratios and minimum drag-due-to-lift factors were found with wings having a $(\beta \cot \Lambda)_{DES}$ of about 0.75 and a design lift coefficient near 0.08. Comparisons of theoretical predictions with experimental results indicated that the theoretical calculations provide good estimates of lift, drag, and pitching moment when the wing surface is mildly cambered and twisted. For wings with severe camber and twist and a high degree of leading-edge sweep, theoretical calculations give good estimates of lift, fair estimates of pitching moment, but poor estimates of drag.

INTRODUCTION

Theoretical supersonic wing analysis and wind-tunnel investigations (refs. 1 to 3) have shown that high aerodynamic efficiency can be obtained by using camber and twist on wings with subsonic leading edges, that is, leading edges swept aft of the Mach line. This high efficiency is realized with highly swept wings because the thickness drag is reduced and the drag-due-to-lift penalties associated with flat wings of that planform are

minimized or avoided. Subsequent studies, such as reference 4, showed that these camber and twist benefits are also present at speeds somewhat higher and lower than the design velocity. The study of spanwise shearing (raising or lowering the leading edge while preserving chordwise slopes) in reference 5 indicated that the efficiency of cambered and twisted wings could be improved still further and that desirable self-trimming characteristics could be incorporated with a minimum of trim drag.

The highly swept wings that can use camber and twist to advantage do not have the subsonic performance and efficiency traits that are inherent with wings of larger span and higher aspect ratio. Therefore, a compromise wing planform incorporating features of a good supersonic and a good subsonic wing is usually employed. Since compromise is necessary, it is important to know the features which give good supersonic as well as good subsonic performance.

The most important supersonic wing design parameters are thought to be the leading-edge sweep angle which determines whether the leading edge will be subsonic or supersonic at design Mach number and the design lift coefficient which determines the severity or degree of warping of the camber surface. Supersonic linearized theory and design methods currently available provide a rational design and analysis procedure, but do not sufficiently account for real flow phenomena so that optimum design parameters may be chosen.

Recently, the relationship between the leading-edge sweep angle and the design lift coefficient for a design Mach number of 2.6, which is in the range of current interest for supersonic vehicle cruise, was studied analytically and experimentally. Nine wings were built. The wing models had leading-edge sweep angles of 69.44°, 72.65°, and 75.96°. For each sweep angle there were three models with camber surfaces that would theoretically give design lift coefficients of 0, 0.08, and 0.12 at a design attitude. The results of the wind-tunnel tests, an analysis of the reduced data, and a comparison of experimental results with theoretical predictions are presented in this report.

SYMBOLS

A	aspect ratio
b	wing span
c	chord
$\bar{c}$	mean geometric chord

c_R root chord

C_D drag coefficient

C_L lift coefficient

$C_{L_\alpha} = \frac{\partial C_L}{\partial \alpha}$ at $\alpha = 0^o$, per degree

C_m pitching-moment coefficient about $0.25\bar{c}$

L/D lift-drag ratio, C_L/C_D

M Mach number

r body radius

t wing thickness

x distance along longitudinal axis

y distance along spanwise axis

z distance normal to XY-plane

α angle of attack

$\beta = (M^2 - 1)^{1/2}$

$\beta \cot \Lambda = \tan (90^o - \Lambda)/\tan \mu$

Δ increment

θ angle between root chord and wing reference plane

Λ leading-edge sweep angle

μ Mach angle, $\sin^{-1} M^{-1}$

Subscripts:

A	arrow wing
B	body; that is, wing fairing to house strain-gage balance
BAL	strain-gage balance
DES	design condition
F	flat wing
le	leading edge
MAX	maximum
mc	moment center
o	zero-lift condition
T	wing tip
W	warped wing; that is, cambered and twisted wing

MODELS

All nine wings used in the wind-tunnel tests were developed from the basic arrow wing planform shown in figure 1. The wing tips were removed at the 90 percent semispan station because previous reports (refs. 1 and 2) had shown that this region experiences flow and aeroelastic deformation which degrades performance. A Mach-angle slanted tip shape was incorporated into the planform design to eliminate tip effects and thus preserve the optimum loading in that region. The reference area for all models was 1935.48 cm^2 (300 in^2).

A three-loading optimization program (ref. 6) provided the theoretical camber surfaces for the three families of wings. Each member of a family had a leading-edge sweep angle of 69.44°, 72.65°, or 75.96° which corresponds to a value of $(\beta \cot \Lambda)_{DES}$ of 0.6, 0.75, or 0.9 at a design Mach number of 2.6. These idealized camber surfaces were modified to eliminate the root chord singularity, usually found in sharp-apex optimized wings, and to obtain the advantages of semispan shearing (ref. 5).

However, the method of shearing used on these wings differed slightly from that reported in reference 5. The camber surface of a wing with a design lift coefficient of 0.12 was modified and sheared until a practical surface was achieved. Then, the camber surfaces for wings with design lift coefficients equal to 0.0 and 0.08 were obtained by linearly proportioning the Z-ordinates for the camber surface of the wing with a design lift coefficient of 0.12. The lift coefficients of the wings were checked by using a computer program based on the method outlined in reference 7 to analyze the modified camber surfaces. Although some loss in design lift coefficient was noted, it was not large enough to warrant a redesign step.

Circular-arc, sharp leading-edge and trailing-edge airfoils of approximately 3 percent thickness were superimposed symmetrically about the camber surface ordinates to form the wing shapes. The thickness-chord ratios were chosen so that all the wings would have about the same thickness-to-length fraction along a line connecting the 0.667 chord stations of the original arrow wings. This constraint, which induced a structural similarity, gave thickness-chord ratios of 0.03, 0.031642, and 0.03354 for wings whose $(\beta \cot \Lambda)_{DES}$ were 0.6, 0.75, and 0.9, respectively. Additional thickness was faired about the root chord to provide volume for a strain-gage balance. Figure 2 shows a general schematic of the final designs. Tables I and II give values of the significant dimensions of the models and the nondimensionalized ordinates of the camber surfaces.

TEST CONDITIONS

Tests were conducted in the 1.22- by 1.22-meter (4 by 4 foot) high-speed section of the Langley Unitary Plan wind tunnel. Mach numbers of 2.3, 2.6, and 2.96 were used with a stagnation temperature of 338.7 K (150° F) and a Reynolds number per meter of 9.843×10^6. To insure turbulent flow over the wing surface, a number 50 size grit was applied along a 0.16 cm (0.0625 in.) wide band 0.32 cm (0.125 in.) behind and normal to the leading edges. Force, pitching moment, and base pressure data were measured and recorded at each Mach number. Strain-gage accuracy and test-data repeatability established data limitations as follows:

$C_L \pm 0.003$

$C_D \pm 0.0003$

$C_m \pm 0.001$

Measurements and calculations were made in U.S. Customary Units and converted to SI Units. Values are given in both SI and U.S. Customary Units.

DISCUSSION OF RESULTS

Wind-tunnel data from the nine wings at Mach numbers of 2.3, 2.6, and 2.96 are shown in figures 3 to 11. The data were corrected to zero base drag conditions. No corrections were made to account for grit drag since this was assumed to be negligibly small and well within the accuracy limits of the instrumentation.

These data were analyzed for two purposes. First and more important, this study shows the effects of the leading-edge sweep angle and the design-lift-coefficient variation on the aerodynamic performance of slightly modified arrow wings. Second, the study compares the theoretical performance of the wings with the wind-tunnel performance of the models.

In figure 12, the lift-curve slope at zero angle of attack and the longitudinal stability derivative at zero lift are shown as functions of the Mach-number—sweep-angle parameter $\beta \cot \Lambda$. The agreement between the theoretical and experimental data for both the lift slope and the longitudinal stability derivative is reasonably good over the range of sweep angles and Mach numbers used in the tests.

A comparison of predicted and measured lift coefficients at design attitude is made in figure 13. The modifications to the optimized camber surfaces produced wings for which the lift coefficient at design attitude and Mach number is close to, but not equal to, the design lift coefficient except for the flat wings where the design lift coefficient is zero. These modifications which were made to obtain practical wing camber surfaces are seen to be minor.

The experimental results from these models which were built from modified camber surface ordinates show good agreement with the theoretical predictions. This agreement indicates that the computer programs, based on references 6 and 7, provide good lift estimates in the test Mach number range.

The pitching-moment coefficient at zero lift is examined in figure 14. Good agreement between predicted and measured values is not found. Since the predicted and the measured values of the stability parameter $\partial C_m/\partial C_L$ agree reasonably well as shown in figure 12(b), satisfactory pitching-moment estimates can be expected, especially in the range from design lift coefficient to lift coefficient at $(L/D)_{MAX}$.

When properly applied, camber and twist reduces the drag due to lift and/or the trim drag of a wing. Supersonic drag is composed of wave or form drag, skin-friction drag, and lift-induced drag. Within linear theory assumptions, wave drag and skin-friction drag are independent of lift and are fixed once the planform and thickness are set. Therefore, the aerodynamic efficiency is improved by reducing the drag-due-to-lift factor.

The usual measure of drag due to lift is $\Delta C_D/\Delta C_L^2$ which is calculated from

$$\Delta C_D/\Delta C_L^2 = \left(C_{D,W} - C_{D,F,o}\right)/C_L^2$$

where $C_{D,W}$ is the drag coefficient of the cambered and twisted wing at some C_L value and $C_{D,F,o}$ is the drag coefficient of the flat wing with the same planform at zero lift. The drag due to lift $\Delta C_D/\Delta C_L^2$ for the nine wings at a Mach number of 2.6 is shown as a function of design lift coefficient in figure 15. Each of the data curves reaches a minimum near a design lift coefficient of 0.08.

In figure 16, several curves are presented for $\Delta C_D/\Delta C_L^2$ as a function of the Mach-number—sweep-angle parameter $(\beta \cot \Lambda)_{DES}$. The topmost curve is the experimental flat-plate $\left(\Delta C_D/\Delta C_L^2 = C_{L_\alpha}^{-1}\right)$ line through the points in figure 15 for which $C_{L,DES} = 0$. Below it is the curve passing through the minimum points on each $(\beta \cot \Lambda)_{DES}$ plot in figure 15. The bottom two curves show the theoretical values of $\Delta C_D/\Delta C_L^2$ for both the wings as built and for the ideal wings having a three-loading optimized camber surface.

The theoretically attainable camber and twist benefits are represented by the gap between the flat-plate $\Delta C_D/\Delta C_L^2$ (the topmost curve) and the optimum-wing $\Delta C_D/\Delta C_L^2$ (the bottom curve). In theory these benefits are substantially realized, but in the wind-tunnel tests they vary from a minimum at $(\beta \cot \Lambda)_{DES}$ of 0.9 to a maximum of about 46 percent at $(\beta \cot \Lambda)_{DES}$ of 0.75.

A more direct method of evaluating the ability of theory to predict drag is to compare the drag polars. Figure 17 shows theoretical and experimental polars of the nine wings at a Mach number of 2.6. The wave and skin-friction drags are assumed to be identical for wings with the same $(\beta \cot \Lambda)_{DES}$. Then the theoretical polar values can be calculated by adding the total wave and skin-friction drag value, which is the measured drag of the flat wings at zero lift, to the theoretical drag-due-to-lift contribution.

A comparison of values for the predicted and measured drag polars shows that theory predicts the drag of the flat wings reasonably well, but as the design lift coefficient increases, the correlation between theoretical predictions and experimental results becomes increasingly poor. If the curves showing the theoretical values predicted for the cambered and twisted wing were shifted along lines of constant C_D, a better agreement between theoretical data and experimental results would be obtained. However, there are no justifications within linear theory for such a shift. A similar lack of measured and predicted polar correlation with wings designed for maximum efficiency at a Mach number of 2.0 is found in figure 7 of reference 1.

The most important factors in the evaluation of aerodynamic efficiency are the lift-drag ratio and the conditions at which it occurs. In figure 18, $(L/D)_{MAX}$ is shown as

a function of Mach number, Mach-number—sweep-angle parameter, and design lift coefficient.

Figure 18(a) shows the performance of the three supersonic wing families across the test Mach number range. In general, the behavior of each wing is similar to that of its counterparts at the other two sweep angles. At the design Mach number when the design lift coefficient was 0.08, the cambered and twisted wings were superior to the flat wings, but when the design lift coefficient was 0.12, only the wing with $(\beta \cot \Lambda)_{DES} = 0.6$ was superior.

The flat wing performance, as shown in figure 18(a), is virtually independent of Mach number except for that of the wing with $(\beta \cot \Lambda)_{DES}$ equal to 0.9. When all the flat wing data are grouped together, as shown in figure 18(b), a peak is found near a $(\beta \cot \Lambda)_{DES}$ of 0.75. Maximums on the curves for the camber and twisted wings show shifts toward lower values of $(\beta \cot \Lambda)_{DES}$. Thus, a peak $(L/D)_{MAX}$ can be maintained while increasing the leading-edge sweep angle if the design lift coefficient is also increased.

However, camber and twist cannot be applied without restraint. A third plot, with $(L/D)_{MAX}$ as a function of $C_{L,DES}$, is shown in figure 18(c). The curves indicate that only a small-to-moderate amount of camber and twist is necessary to improve the efficiency of a flat wing. Increasing the camber surface severity beyond what is needed to obtain a $C_{L,DES}$ of about 0.08 results in a decreasing $(L/D)_{MAX}$ and, as is shown in figure 15, an increasing $\Delta C_D/\Delta C_L{}^2$.

Although maximum lift-drag ratio is the major factor in evaluating wing efficiency, it is also necessary to know the lift coefficient, the angle of attack, and the pitching moment at $(L/D)_{MAX}$. In figure 19, these quantities are shown as functions of $C_{L,DES}$ at the design Mach number of 2.6. The lift-coefficient curves are well separated and almost parallel, whereas, for the most part, the angle-of-attack and the pitching-moment-coefficient curves are two narrow bands across the $C_{L,DES}$ range. In going from a $C_{L,DES}$ of 0.0 to 0.08, where the $(L/D)_{MAX}$ appears to peak, the available lift increases about 12 percent and the angle of attack decreases about 2.5°. Thus, aerodynamic efficiency is increased by reducing, though not necessarily eliminating, the flat-wing lift component.

A comparison of predicted and measured maximum lift-drag ratios is shown in figure 20. The theoretical results in this study and in reference 1 indicate that the highest levels of $(L/D)_{MAX}$ should be found when the wings are severely cambered and twisted. However, the experimental data from both studies demonstrate that moderate warping, or enough camber and twist to obtain a $C_{L,DES}$ of about 0.08, produces the more efficient wings.

CONCLUSIONS

The effects of varying the leading-edge sweep angle and the design lift coefficient were studied in wind-tunnel tests on nine wing models. The experimental data were analyzed and compared with theoretical calculations. The following conclusions were drawn from this study:

1. Flat wing maximum lift-drag ratios increase as the leading edge is swept aft of the Mach line. A peak value is reached near a $(\beta \cot \Lambda)_{DES}$ of 0.75 at the design Mach number of 2.6 as well as at the two off-design Mach numbers of 2.3 and 2.96.

2. Maximum lift-drag ratios of the cambered and twisted wings peak at $(\beta \cot \Lambda)_{DES}$ values which are less than 0.75. Moreover, the value of $(\beta \cot \Lambda)_{DES}$ at which the maximum lift-drag ratios occur decreases as the design lift coefficient is increased. At a design Mach number of 2.6, these ratios are found between design lift coefficients of 0.04 and 0.08.

3. When the wings are cambered and twisted for a design lift coefficient of 0.08 at a Mach number of 2.6, the available lift at maximum lift-drag ratios is about 12 percent greater than the available flat-wing lift.

4. For the Mach number range of the study, supersonic linear theory is capable of providing good estimates of lift, drag, and pitching moment for flat-plate wings and for wings with moderate camber surfaces. However, for highly swept wings with more severely cambered and twisted surfaces, the theory fails to adequately predict drag levels.

Langley Research Center,
National Aeronautics and Space Administration,
Hampton, Va., October 30, 1974.

REFERENCES

1. Carlson, Harry W.: Aerodynamic Characteristics at Mach Number 2.05 of a Series of Highly Swept Arrow Wings Employing Various Degrees of Twist and Camber. NASA TM X-332, 1960.

2. Carlson, Harry W.: Pressure Distributions at Mach Number 2.05 on a Series of Highly Swept Arrow Wings Employing Various Degrees of Twist and Camber. NASA TN D-1264, 1962.

3. McLean, F. Edward; and Fuller, Dennis E.: Supersonic Aerodynamic Characteristics of Some Simplified and Complex Aircraft Configurations Which Employ Highly Swept Twisted-and-Cambered Arrow-Wing Planforms. Vehicle Design and Propulsion. American Inst. Aeron. and Astronautics, Nov. 1963, pp. 98-103.

4. Middleton, Wilbur D.; and Sorrells, Russell B.: Off-Design Aerodynamic Characteristics at Mach Numbers 1.61 and 2.20 of a Series of Highly Swept Arrow Wings Designed for Mach Number 2.0 Employing Various Degrees of Twist and Camber. NASA TN D-1630, 1963.

5. Landrum, Emma Jean; and Shrout, Barrett L.: Effect of Shape Changes on the Aerodynamic Characteristics of a Twisted and Cambered Arrow Wing at Mach Number 2.03. NASA TN D-4796, 1968.

6. Carlson, Harry W.; and Middleton, Wilbur D.: A Numerical Method for the Design of Camber Surfaces of Supersonic Wings With Arbitrary Planforms. NASA TN D-2341, 1964.

7. Middleton, Wilbur.; and Carlson, Harry W.: A Numerical Method for Calculating the Flat-Plate Pressure Distributions on Supersonic Wings of Arbitrary Planform. NASA TN D-2570, 1965.

TABLE I.- DIMENSIONS OF THE TEST MODELS

	$(\beta \cot \Lambda)_{DES}$ of –		
	0.6	0.75	0.9
Λ, deg	75.96	72.65	69.44
A	1.101	1.374	1.647
b/2, cm	23.033	25.786	28.232
$\bar{c}$, cm	52.08	46.515	42.415
c_R, cm	76.926	68.76	62.738
x_B, cm	80.01	71.12	66.04
x_{BAL}, cm	63.500	56.896	52.07
x_{MAX}, cm	97.743	87.668	80.195
x_{mc}, cm	46.147	41.29	37.702
x_T, cm	92.314	82.512	75.286
y_{mc}, cm	8.282	9.269	10.162
$y(x_{MAX})$, cm	20.815	23.637	26.187
t/c	0.0300	0.03164	0.03354
	$C_{L,DES}$ of –		
	0	0.08	0.12
θ, deg	0	6	9

TABLE II.- CAMBER SURFACE ORDINATES

(a) $(\beta \cot \Lambda)_{DES} = 0.6$ wings

$\frac{y}{b/2}$	$(z/x_{MAX})C_{L,DES}$ for $\frac{x - x_{le}}{c}$ of –												
	0.0000	.0500	.1000	.1500	.2000	.3000	.4000	.5000	.6000	.7000	.8000	.9000	1.0000
0.0000	.6627	.6107	.5587	.5067	.4548	.3509	.2469	.1429	.0387	-.0653	-.1692	-.2732	-.3768
.0220	.6035	.5944	.5334	.4824	.4314	.3294	.2274	.1257	.0237	-.0783	-.1803	-.2820	-.3840
.0440	.5444	.5165	.5022	.4580	.4080	.3083	.2082	.1085	.0084	-.0913	-.1910	-.2910	-.3908
.0660	.4889	.4704	.4437	.4025	.3775	.2868	.1891	.0913	-.0065	-.1043	-.2020	-.2998	-.3976
.0880	.4344	.4242	.4044	.3680	.3222	.2313	.1410	.0507	-.0380	-.1195	-.2131	-.3089	-.4044
.1000	.4050	.3994	.3833	.3493	.3053	.2166	.1278	.0390	-.0476	-.1321	-.2166	-.2880	-.3551
.1500	.2880	.2984	.2967	.2746	.2404	.1663	.0866	.0065	-.0715	-.1485	-.2220	-.2837	-.3404
.2000	.1949	.2098	.2144	.2016	.1775	.1200	.0546	-.0130	-.0812	-.1490	-.2144	-.2718	-.3248
.3000	.0747	.0983	.1107	.1045	.0886	.0574	.0162	-.0349	-.0799	-.1306	-.1817	-.2285	-.2761
.4000	.0204	.0439	.0587	.0593	.0520	.0347	.0076	-.0249	-.0639	-.1016	-.1407	-.1787	-.2159
.5000	0.0000	.0241	.0407	.0448	.0422	.0347	.0162	-.0043	-.0325	-.0585	-.0888	-.1180	-.1494
.6000	0.0000	.0225	.0390	.0456	.0465	.0455	.0360	.0243	.0087	-.0076	-.0314	-.0520	-.0723
.7000	0.0000	.0180	.0325	.0411	.0455	.0487	.0477	.0416	.0325	.0238	.0102	-.0022	-.0172
.8000	0.0000	.0139	.0260	.0349	.0412	.0485	.0520	.0498	.0477	.0433	.0399	.0268	.0260
.9000	0.0000	.0083	.0162	.0237	.0310	.0433	.0481	.0516	.0541	.0552	.0559	.0543	.0524
1.0000	0.0000	0.0000	0.0000	0.0000	0.0000	0.0000	0.0000	0.0000	0.0000	0.0000	0.0000	0.0000	0.0000

TABLE II.- CAMBER SURFACE ORDINATES – Continued

(b) $(\beta \cot \Lambda)_{DES} = 0.75$ wings

$\frac{y}{b/2}$	$(z/x_{MAX})C_{L,DES}$ for $\frac{x - x_{le}}{c}$ of –												
	0.0000	.0500	.1000	.1500	.2000	.3000	.4000	.5000	.6000	.7000	.8000	.9000	1.0000
0.0000	.7413	.6896	.6378	.5860	.5342	.4306	.3274	.2238	.1202	.0167	-.0869	-.1905	-.2941
.0197	.6588	.6425	.6153	.5642	.5125	.4118	.3100	.2082	.1068	.0051	-.0967	-.1985	-.3002
.0394	.5766	.5443	.5088	.5190	.4882	.3929	.2930	.1930	.0931	-.0065	-.1065	-.2064	-.3060
.0591	.5020	.4795	.4513	.4139	.4063	.3531	.2734	.1778	.0797	-.0181	-.1163	-.2144	-.3122
.0788	.4357	.4205	.3991	.3665	.3270	.2452	.1934	.1130	.0272	-.0536	-.1260	-.2224	-.3183
.0887	.4027	.3911	.3730	.3426	.3053	.2263	.1449	.0623	-.0159	-.0960	-.1659	-.2267	-.2850
.1000	.3646	.3575	.3429	.3155	.2801	.2040	.1256	.0459	-.0290	-.1062	-.1726	-.2294	-.2837
.1500	.2487	.2500	.2438	.2252	.1980	.1364	.0724	.0084	-.0579	-.1243	-.1787	-.2270	-.2801
.2000	.1690	.1756	.1750	.1622	.1412	.0917	.0386	-.0145	-.0724	-.1280	-.1738	-.2185	-.2668
.3000	.0564	.0800	.0857	.0785	.0640	.0290	-.0060	-.0471	-.0881	-.1268	-.1654	-.2040	-.2426
.4000	.0205	.0319	.0386	.0373	.0302	.0097	-.0145	-.0483	-.0772	-.1098	-.1388	-.1690	-.1980
.5000	0.0000	.0116	.0193	.0206	.0181	.0097	-.0097	-.0314	-.0531	-.0772	-.1014	-.1231	-.1449
.6000	0.0000	.0112	.0193	.0223	.0229	.0229	.0121	-.0036	-.0181	-.0350	-.0531	-.0688	-.0869
.7000	0.0000	.0108	.0193	.0240	.0265	.0302	.0265	.0193	.0097	0.0000	-.0145	-.0254	-.0386
.8000	0.0000	.0105	.0193	.0252	.0290	.0338	.0338	.0314	.0290	.0229	.0145	.0084	0.0000
.9167	0.0000	.0089	.0159	.0198	.0222	.0271	.0290	.0309	.0314	.0314	.0300	.0290	.0280
1.0000	0.0000	0.0000	0.0000	0.0000	0.0000	0.0000	0.0000	0.0000	0.0000	0.0000	0.0000	0.0000	0.0000

TABLE II.- CAMBER SURFACE ORDINATES – Concluded

(c) $(\beta \cot \Lambda)_{DES} = 0.9$ wings

$\frac{y}{b/2}$	$(z/x_{MAX})C_{L,DES}$ for $\frac{x - x_{le}}{c}$ of –												
	0.0000	.0500	.1000	.1500	.2000	.3000	.4000	.5000	.6000	.7000	.8000	.9000	1.0000
0.0000	.7839	.7324	.6806	.6291	.5772	.4743	.3710	.2676	.1643	.0610	-.0424	-.1453	-.2486
.0180	.6794	.6346	.6473	.6093	.5582	.4569	.3551	.2538	.1520	.0503	-.0511	-.1528	-.2542
.0360	.5749	.5388	.5006	.5270	.4996	.4239	.3397	.2395	.1298	.0400	-.0602	-.1599	-.2597
.0540	.4798	.4517	.4201	.3832	.3440	.3559	.2894	.2090	.1267	.0293	-.0689	-.1671	-.2657
.0720	.4189	.3951	.3682	.3361	.3013	.2364	.1928	.1338	.0554	-.0194	-.0863	-.1746	-.2712
.0810	.3880	.3666	.3425	.3128	.2799	.2106	.1362	.0626	-.0099	-.0800	-.1445	-.2015	-.2439
.1000	.3232	.3070	.2877	.2623	.2349	.1715	.1029	.0343	-.0317	-.0977	-.1557	-.2059	-.2428
.1500	.2270	.2170	.2046	.1877	.1663	.1135	.0581	.0013	-.0528	-.1069	-.1584	-.2019	-.2375
.2000	.1597	.1558	.1478	.1327	.1135	.0726	.0277	-.0185	-.0660	-.1122	-.1571	-.1966	-.2323
.3000	.0726	.0742	.0713	.0612	.0475	.0211	-.0106	-.0449	-.0805	-.1148	-.1491	-.1821	-.2164
.4000	.0211	.0242	.0238	.0176	.0079	-.0132	-.0369	-.0607	-.0844	-.1109	-.1386	-.1663	-.1940
.5000	0.0000	.0041	.0053	.0017	-.0053	-.0224	-.0396	-.0554	-.0752	-.0955	-.1161	-.1346	-.1557
.6000	0.0000	.0049	.0066	.0032	-.0013	-.0066	-.0224	-.0343	-.0475	-.0520	-.0765	-.0911	-.1069
.7000	0.0000	.0053	.0079	.0062	.0027	-.0027	-.0106	-.0171	-.0264	-.0369	-.0462	-.0567	-.0673
.8000	0.0000	.0051	.0079	.0072	.0053	.0040	0.0000	-.0066	-.0106	-.0158	-.0211	-.0290	-.0356
.9275	0.0000	.0021	.0037	.0044	.0045	.0045	.0037	.0024	.0008	-.0008	-.0024	-.0040	-.0055
1.0000	0.0000	0.0000	0.0000	0.0000	0.0000	0.0000	0.0000	0.0000	0.0000	0.0000	0.0000	0.0000	0.0000

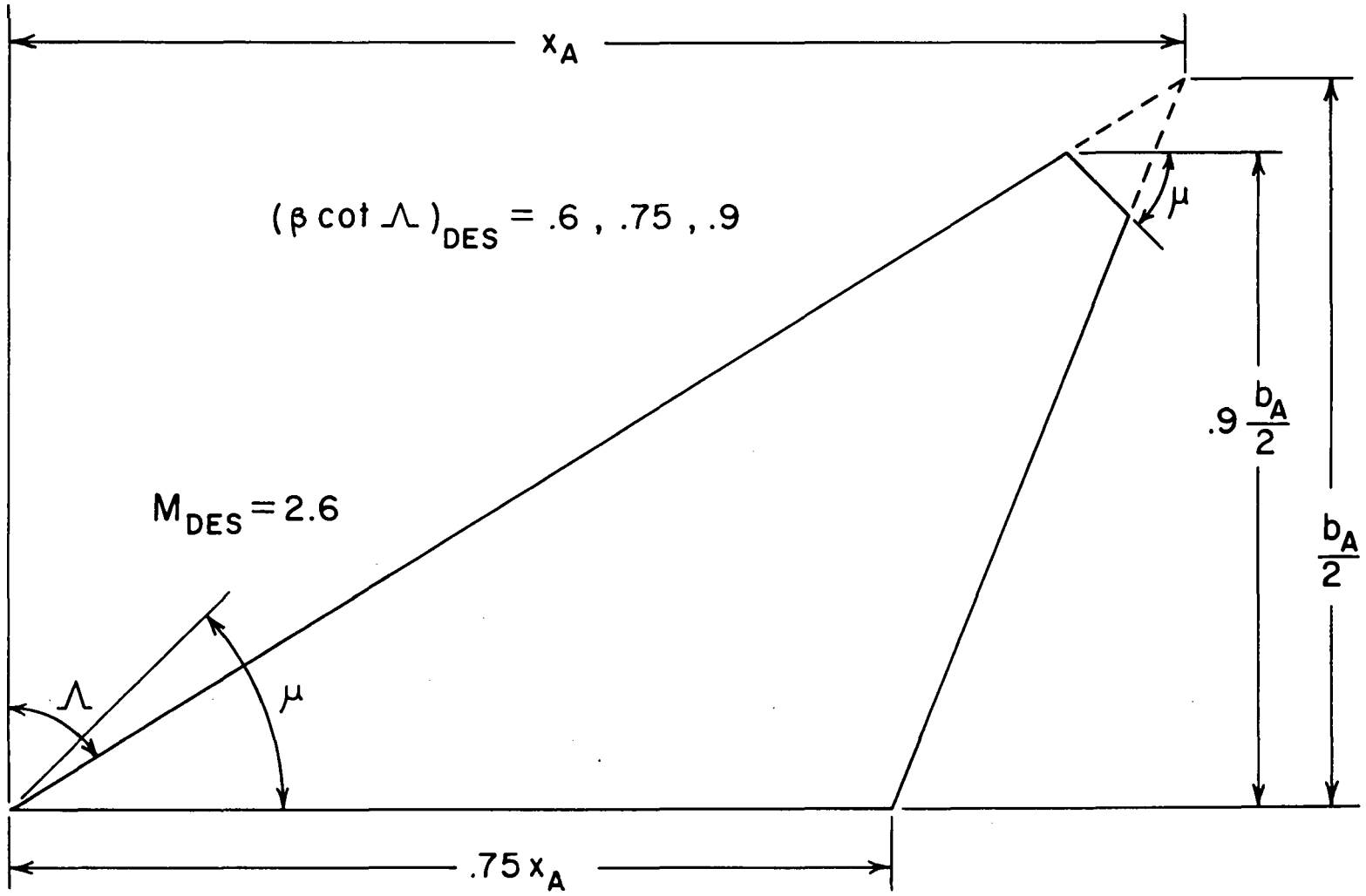

Figure 1.- Development of the wing planform used on the test models.

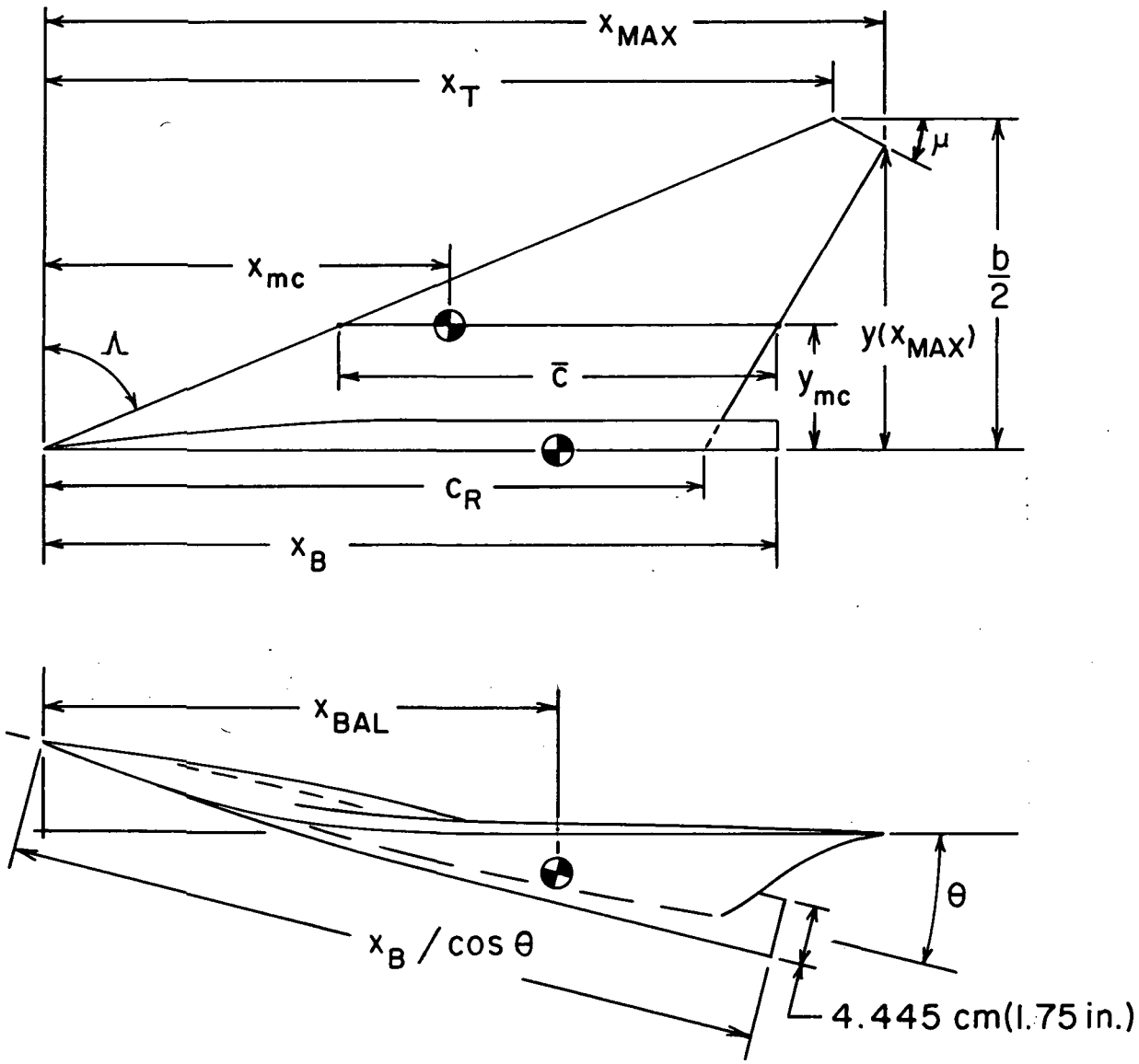

(a) Top and side views of planform.

Figure 2.- Wind-tunnel test model schematic.

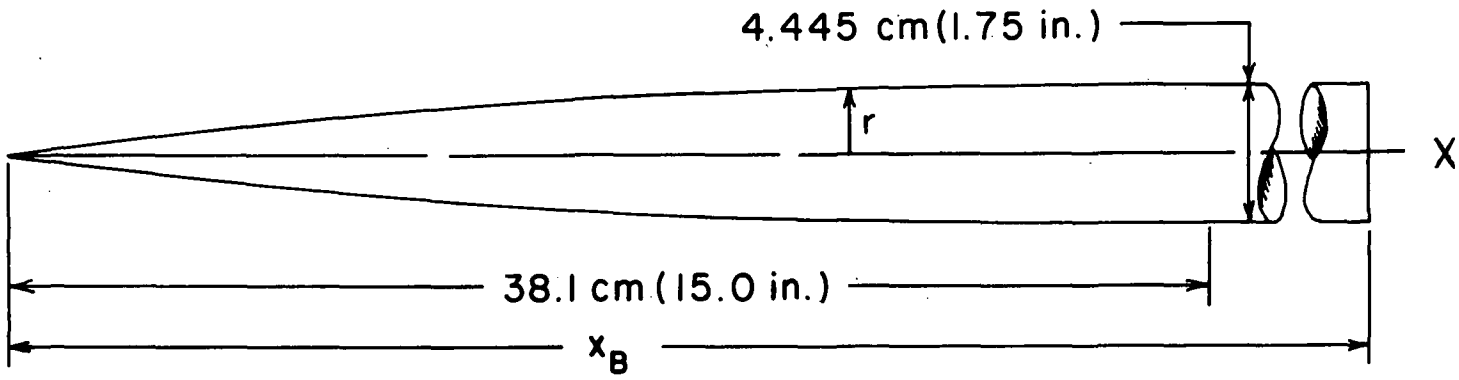

x, cm	0	5	10	15	20	25	30	35	38.1
r, cm	0	.699	.864	1.613	1.880	2.082	2.184	2.220	2.2225

Fairing is cylindrical from 38.1 cm to x_B

(b) Description of root-chord fairing which encloses strain-gage balance.

Figure 2.- Concluded.

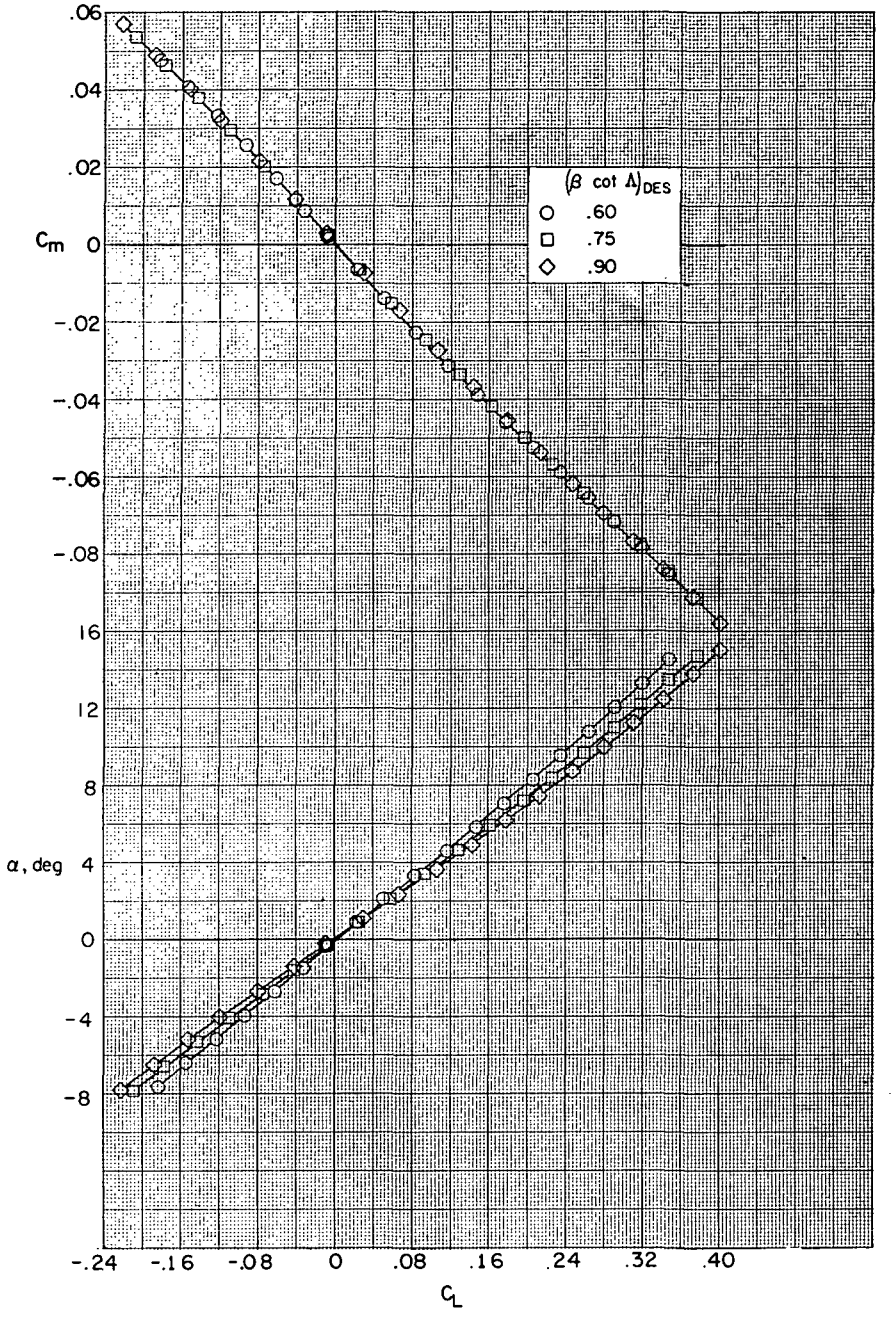

(a) Pitching-moment coefficient and angle of attack as functions of lift coefficient.

Figure 3.- Measured aerodynamic characteristics at $M = 2.3$ of the wings with $C_{L,DES} = 0$.

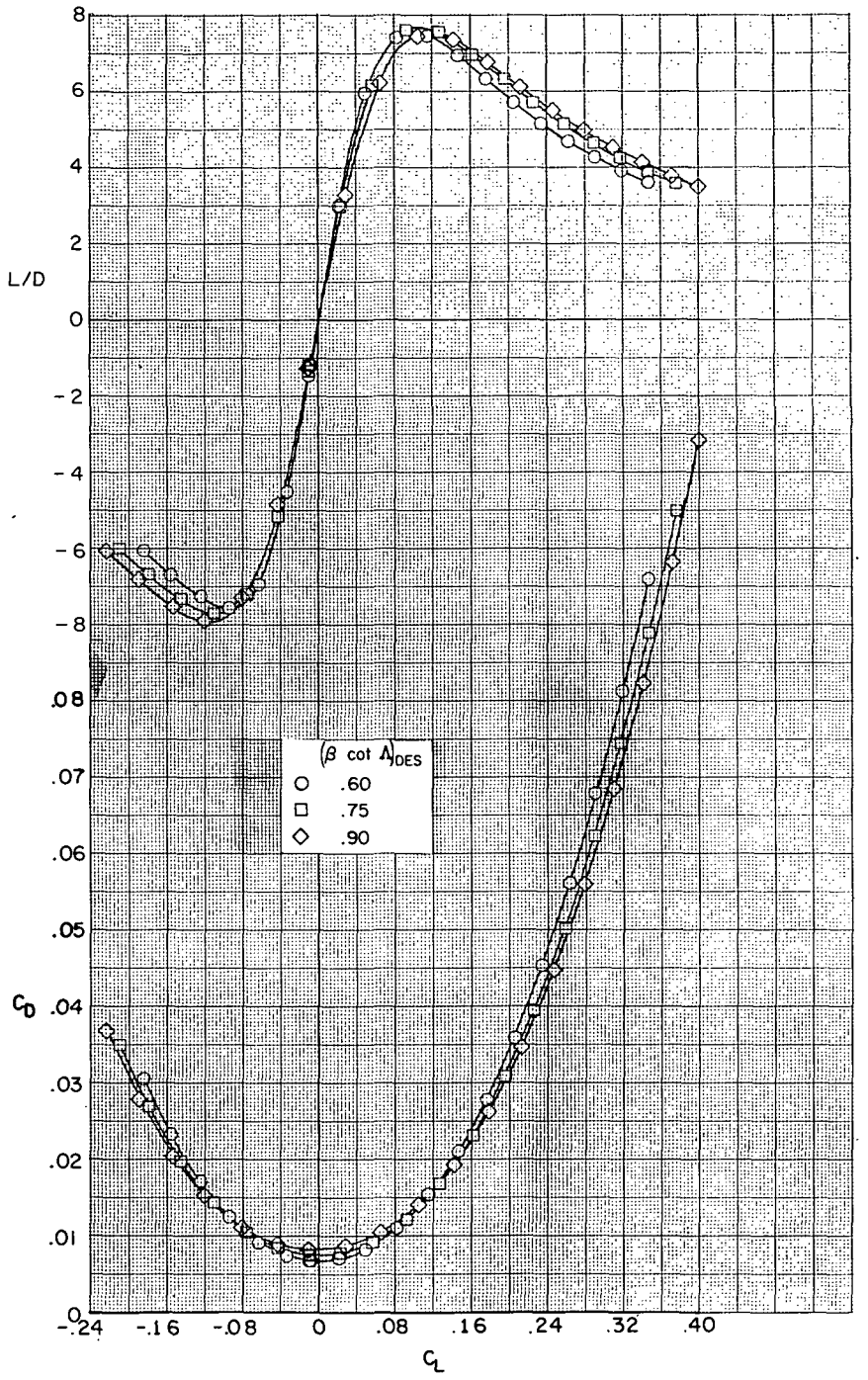

(b) Drag coefficient and lift-drag ratio as functions of lift coefficient.

Figure 3.- Concluded.

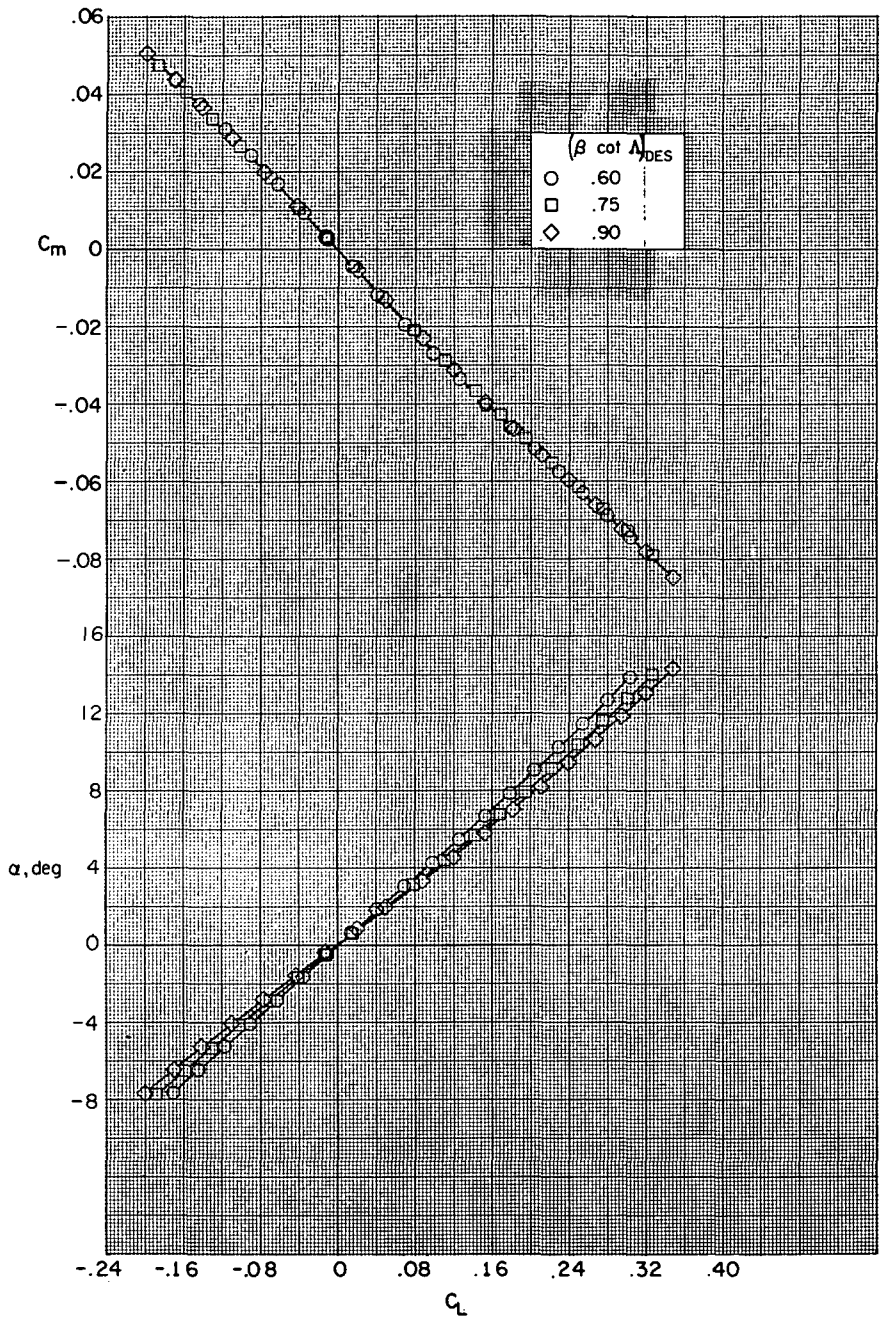

(a) Pitching-moment coefficient and angle of attack as functions of lift coefficient.

Figure 4.- Measured aerodynamic characteristics at M = 2.6 of the wings with $C_{L,DES} = 0$.

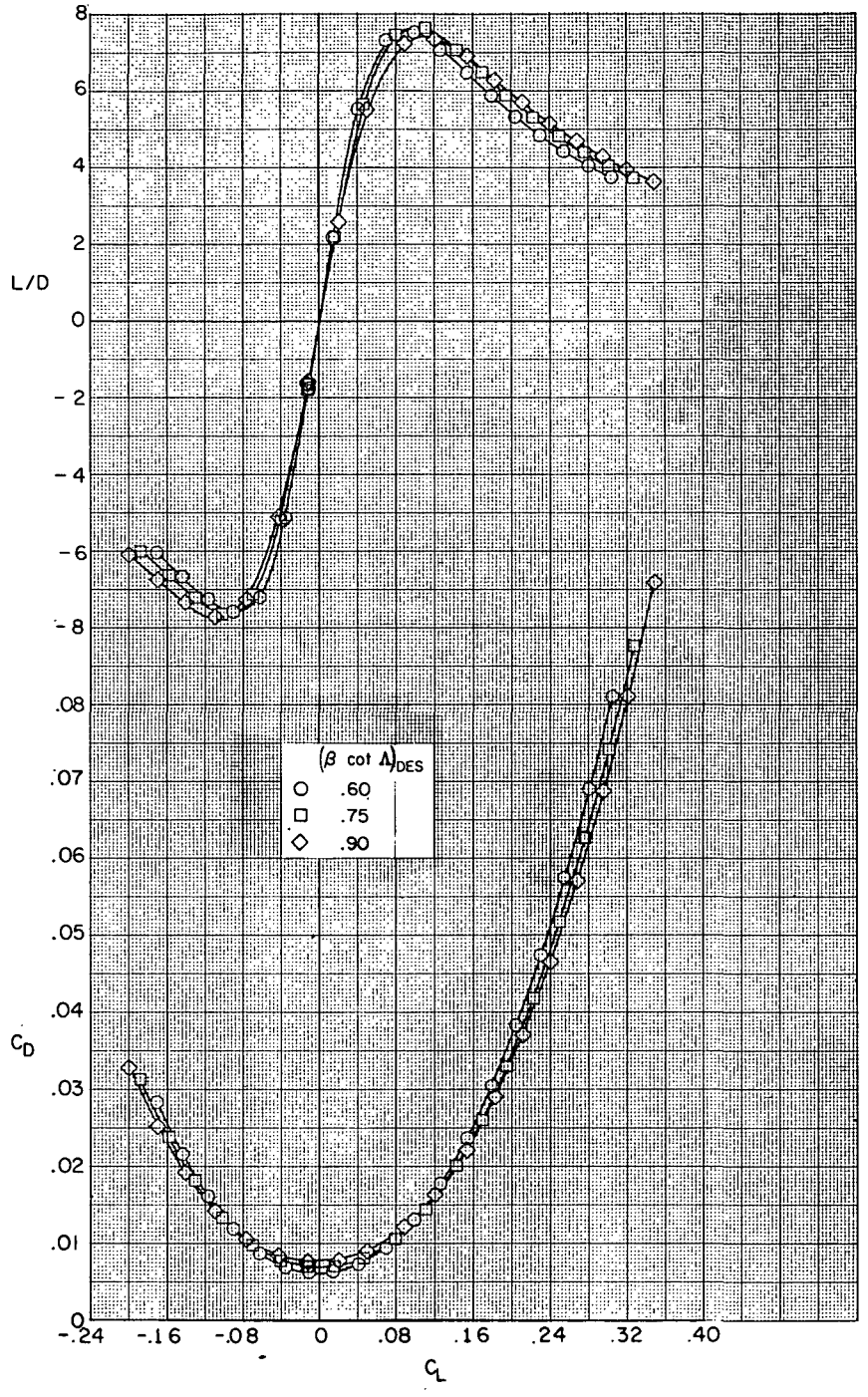

(b) Drag coefficient and lift-drag ratio as functions of lift coefficient.

Figure 4.- Concluded.

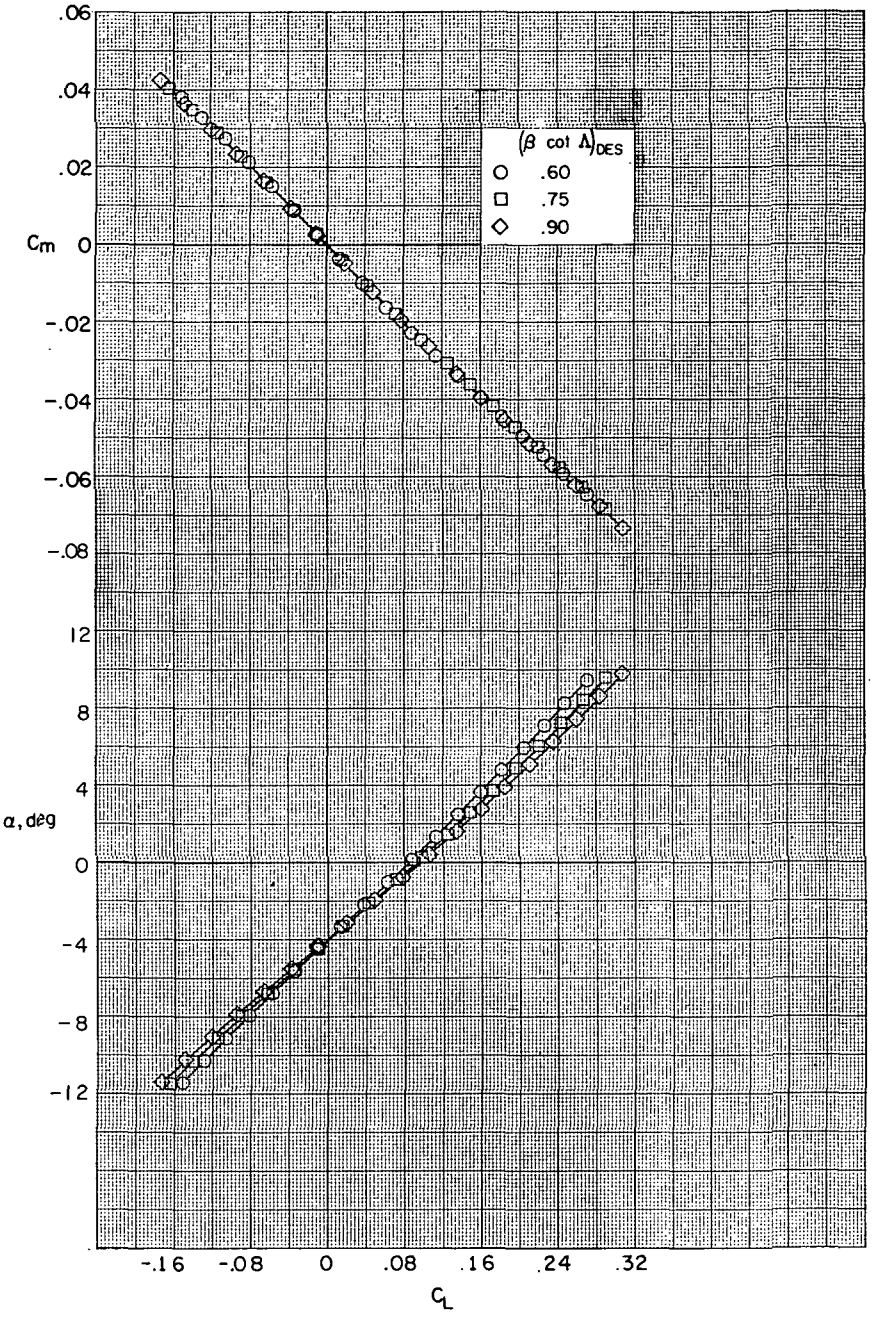

(a) Pitching-moment coefficient and angle of attack as functions of lift coefficient.

Figure 5.- Measured aerodynamic characteristics at M = 2.96 of the wings with $C_{L,DES} = 0$.

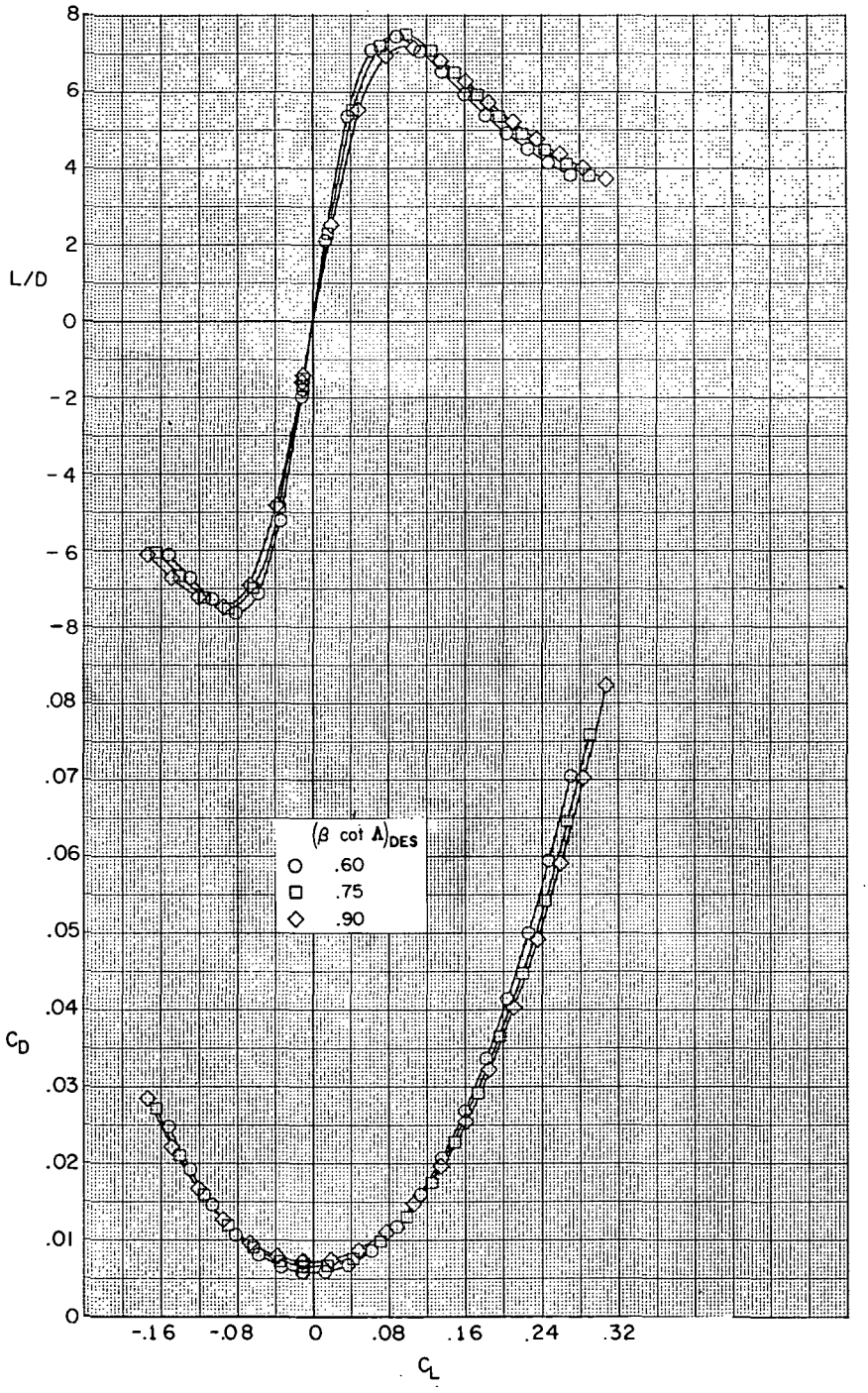

(b) Drag coefficient and lift-drag ratio as functions of lift coefficient.

Figure 5.- Concluded.

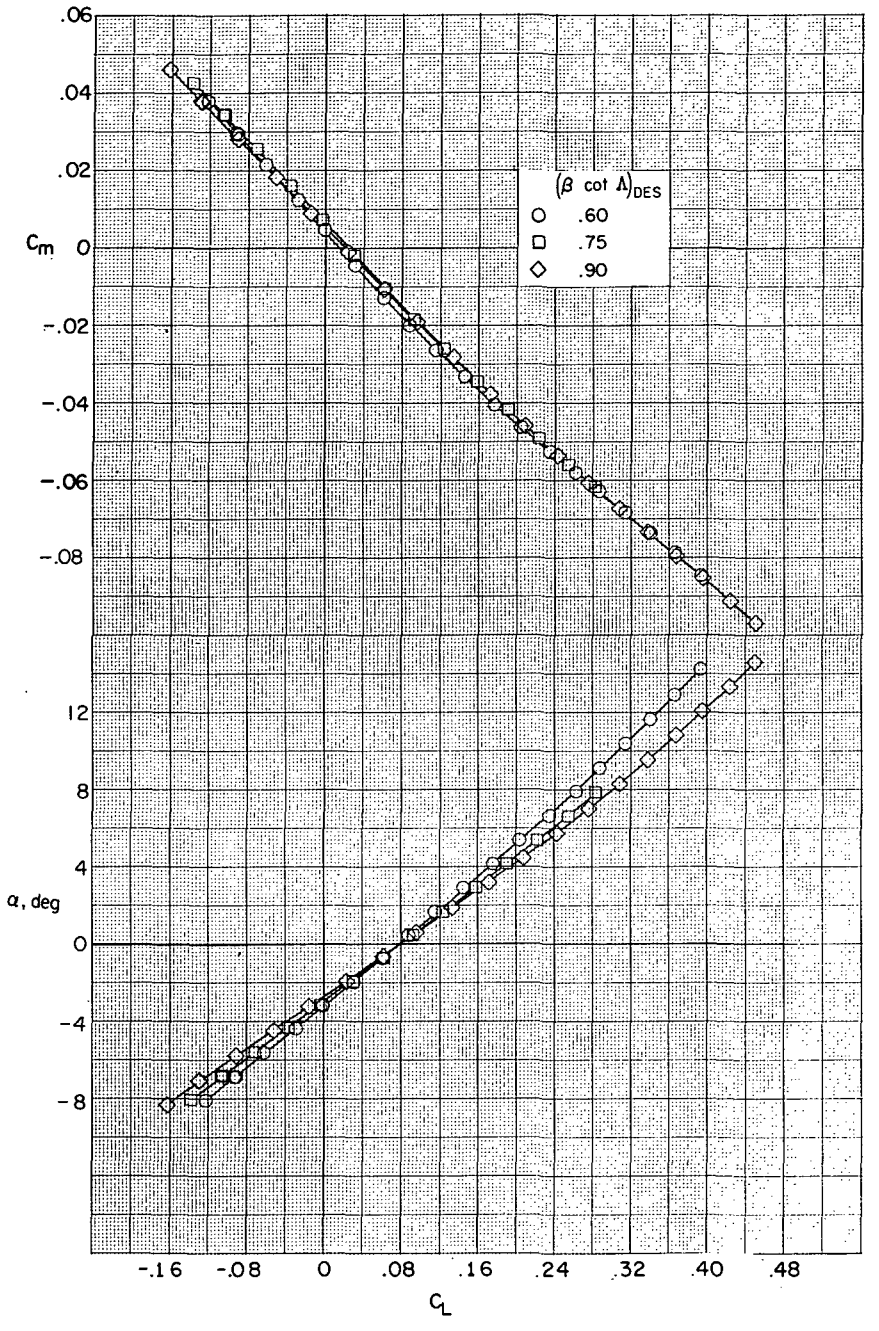

(a) Pitching-moment coefficient and angle of attack as functions of lift coefficient.

Figure 6.- Measured aerodynamic characteristics at $M = 2.3$ of the wings with $C_{L,DES} = 0.08$.

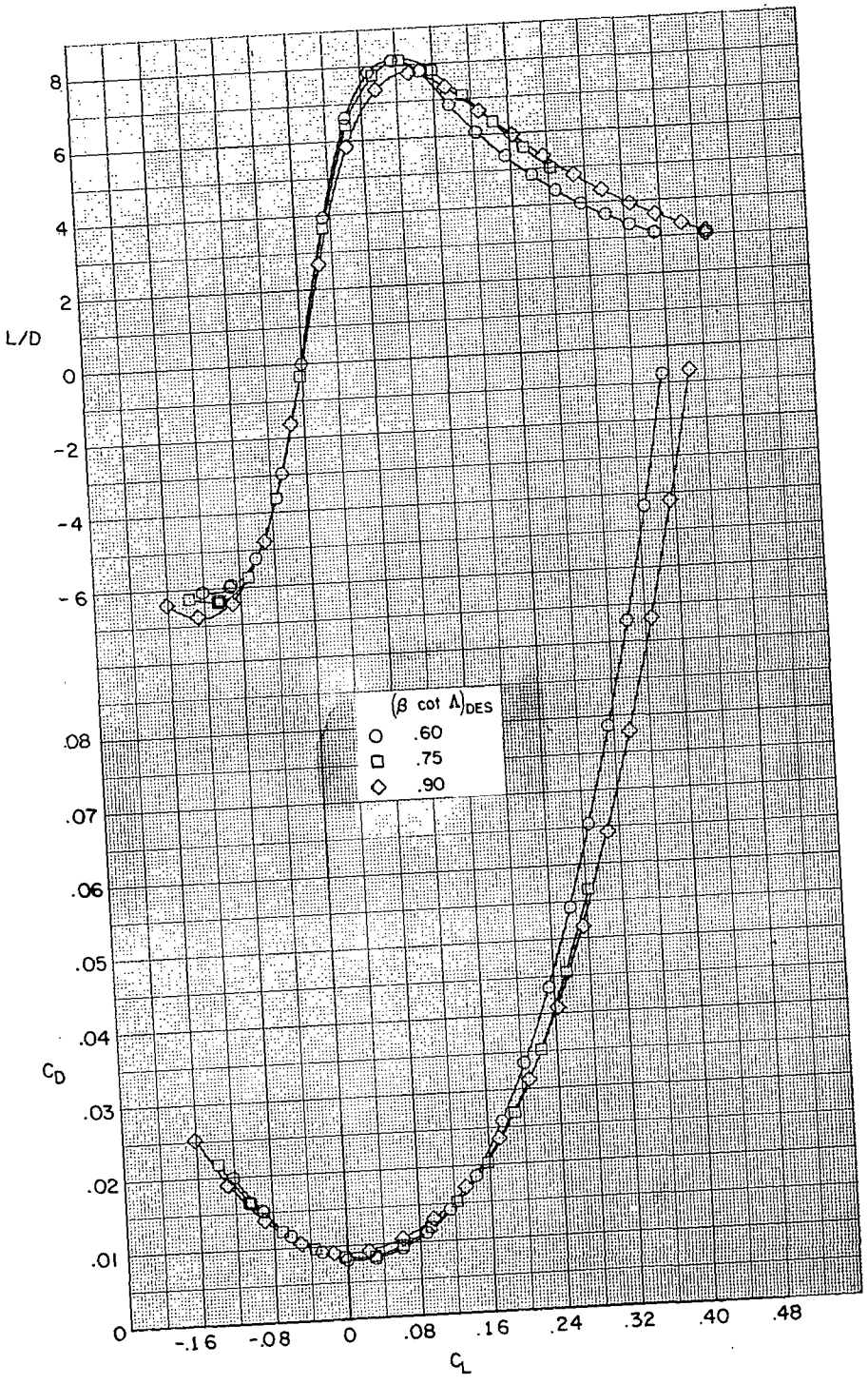

(b) Drag coefficient and lift-drag ratio as functions of lift coefficient.

Figure 6.- Concluded.

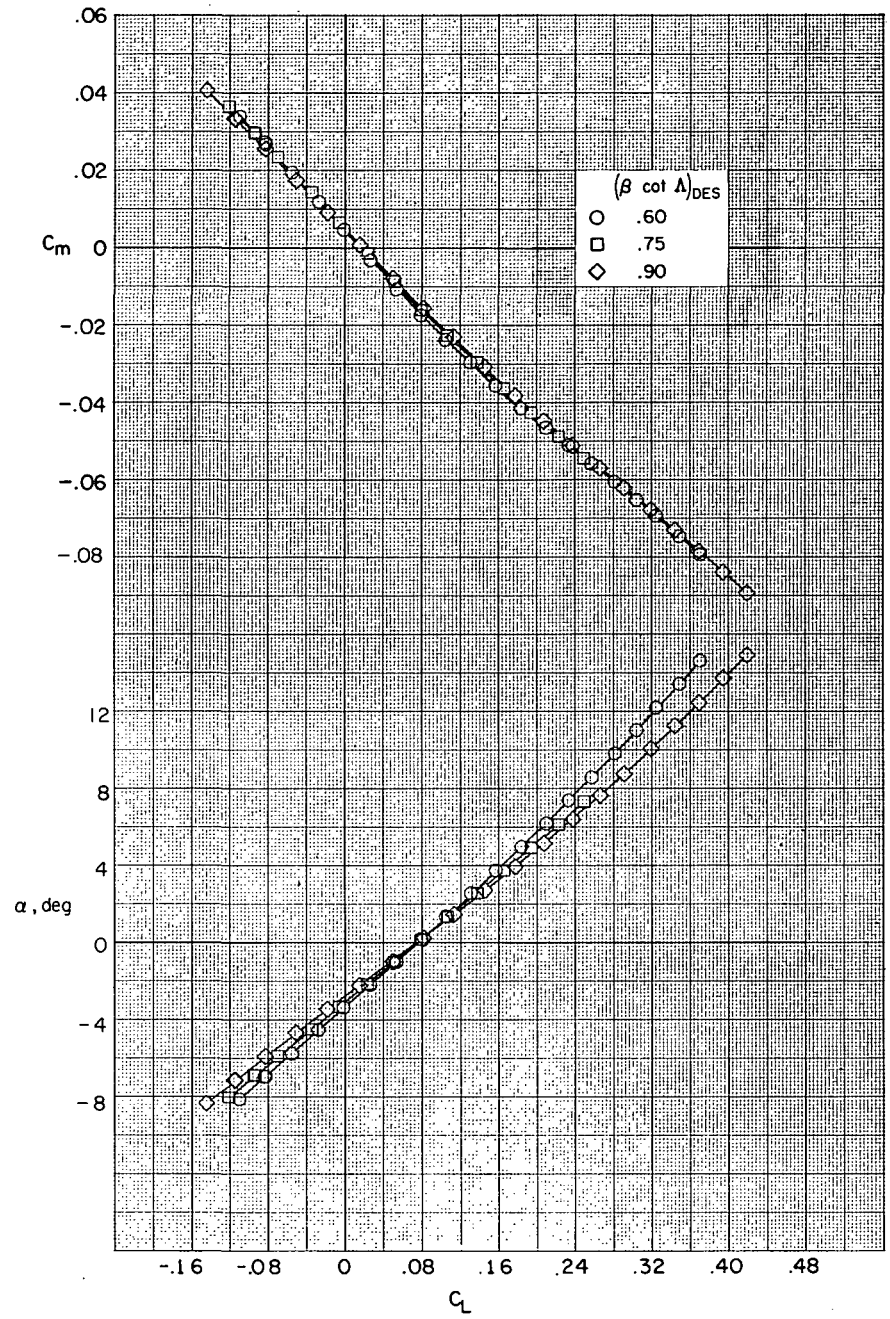

(a) Pitching-moment coefficient and angle of attack as functions of lift coefficient.

Figure 7.- Measured aerodynamic characteristics at $M = 2.6$ of the wings with $C_{L,DES} = 0.08$.

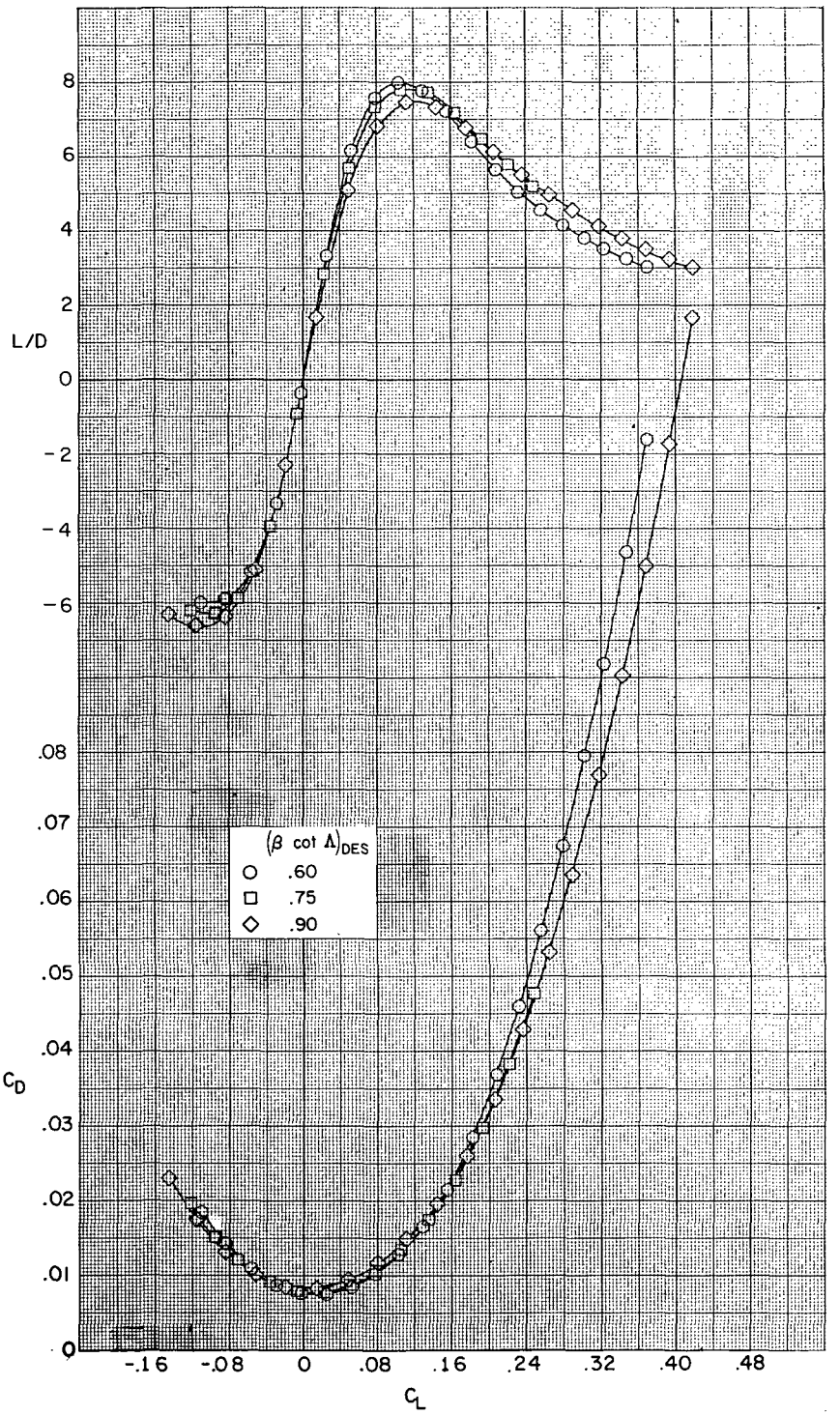

(b) Drag coefficient and lift-drag ratio as functions of lift coefficient.

Figure 7.- Concluded.

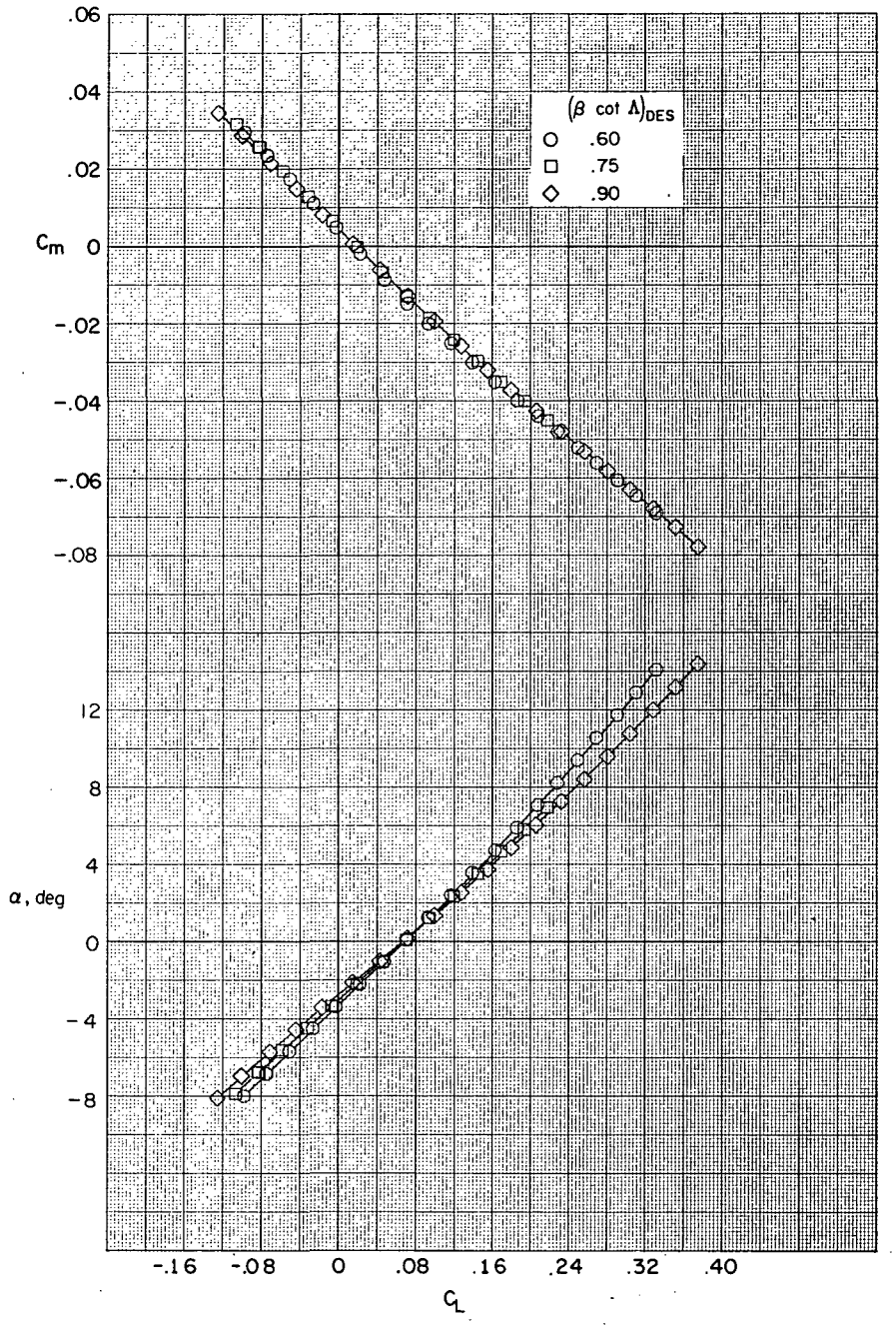

(a) Pitching-moment coefficient and angle of attack as functions of lift coefficient.

Figure 8.- Measured aerodynamic characteristics at M = 2.96 of the wings with $C_{L,DES} = 0.08$.

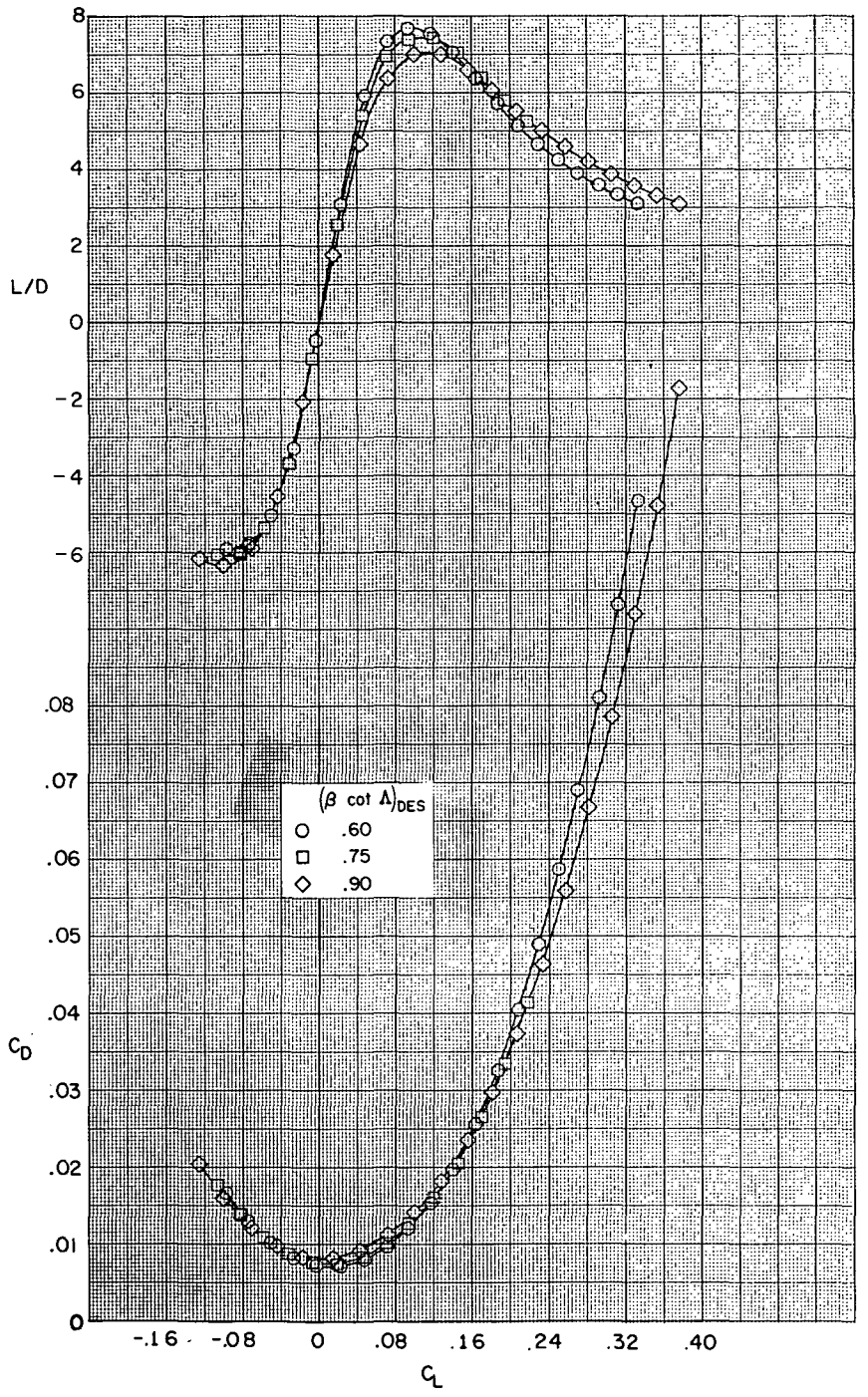

(b) Drag coefficient and lift-drag ratio as functions of lift coefficient.

Figure 8.- Concluded.

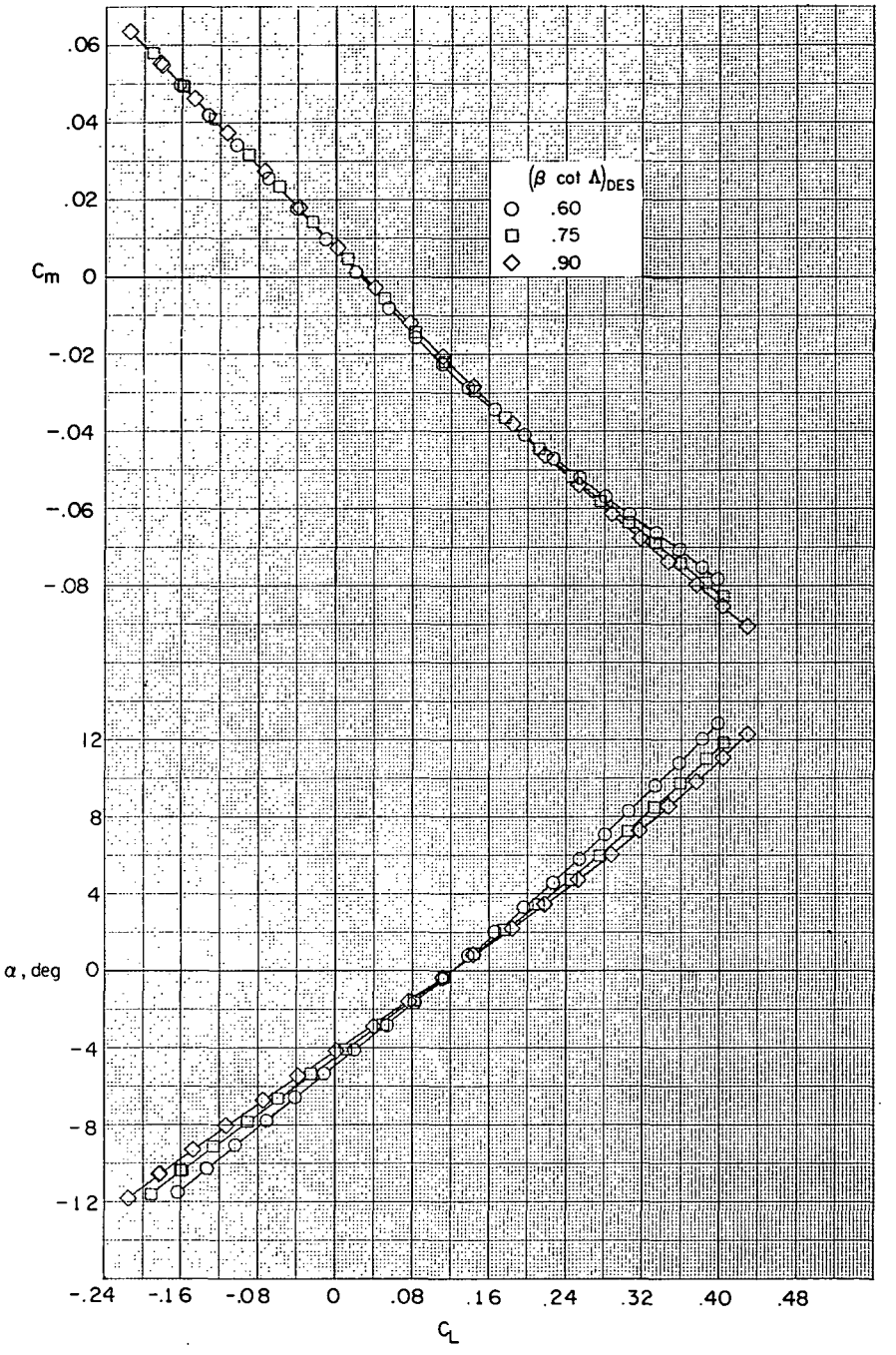

(a) Pitching-moment coefficient and angle of attack as functions of lift coefficient.

Figure 9.- Measured aerodynamic characteristics at M = 2.3 of the wings with $C_{L,DES} = 0.12$.

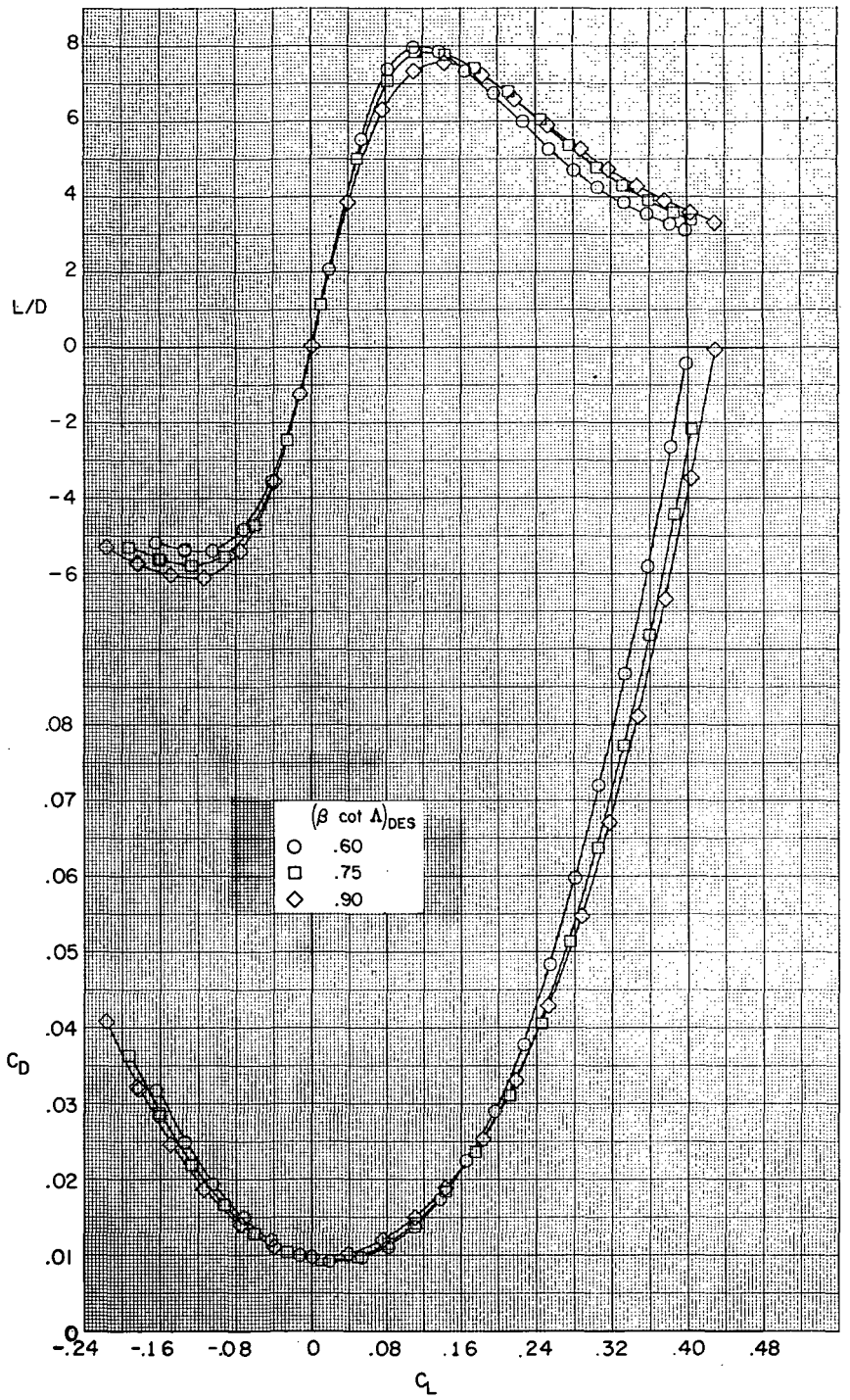

(b) Drag coefficient and lift-drag ratio as functions of lift coefficient.

Figure 9.- Concluded.

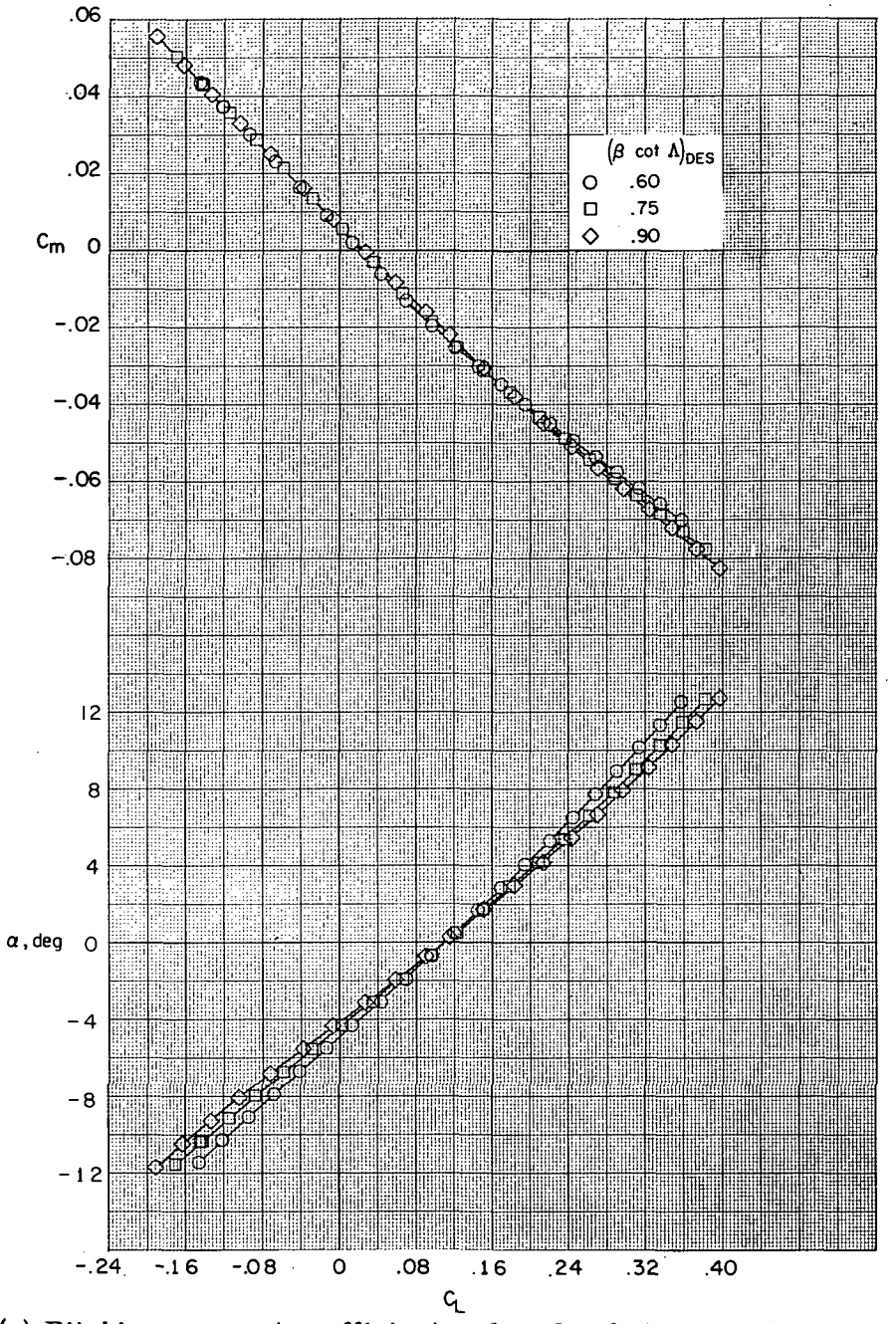

(a) Pitching-moment coefficient and angle of attack as functions of lift coefficient.

Figure 10.- Measured aerodynamic characteristics at M = 2.6 of the wings with $C_{L,DES} = 0.12$.

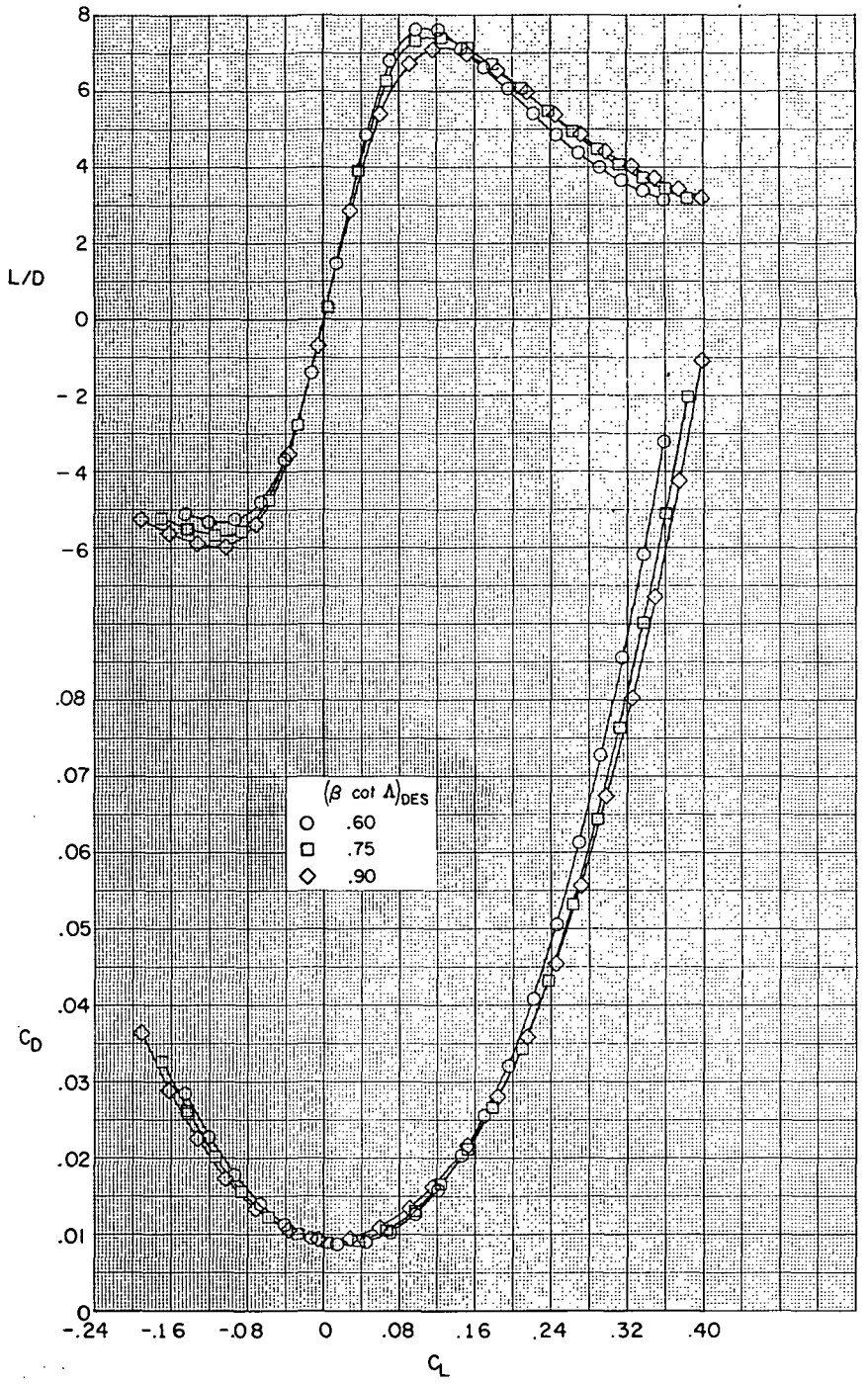

(b) Drag coefficient and lift-drag ratio as functions of lift coefficient.

Figure 10.- Concluded.

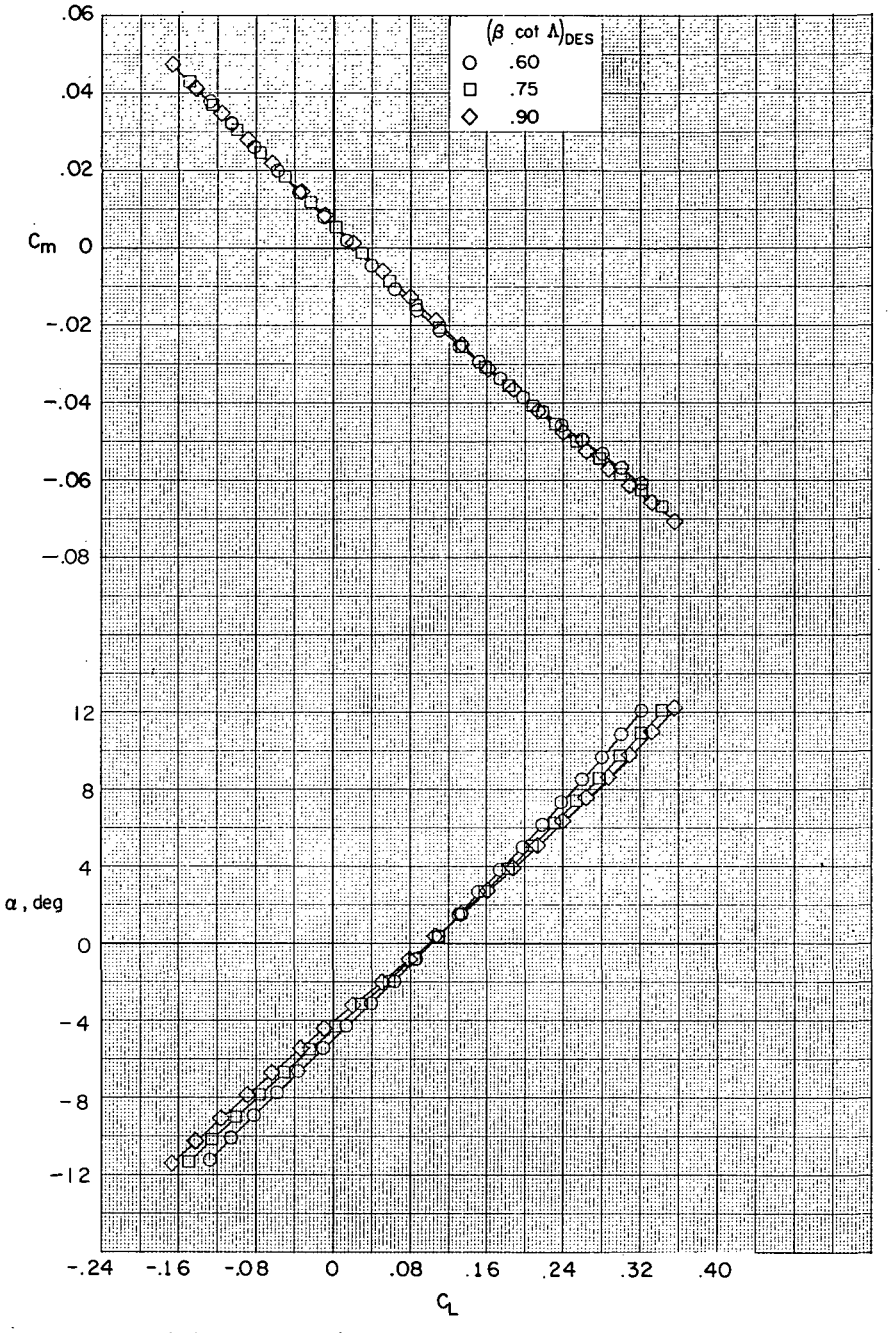

(a) Pitching-moment coefficient and angle of attack as functions of lift coefficient.

Figure 11.- Measured aerodynamic characteristics at M = 2.96 of the wings with $C_{L,DES} = 0.12$.

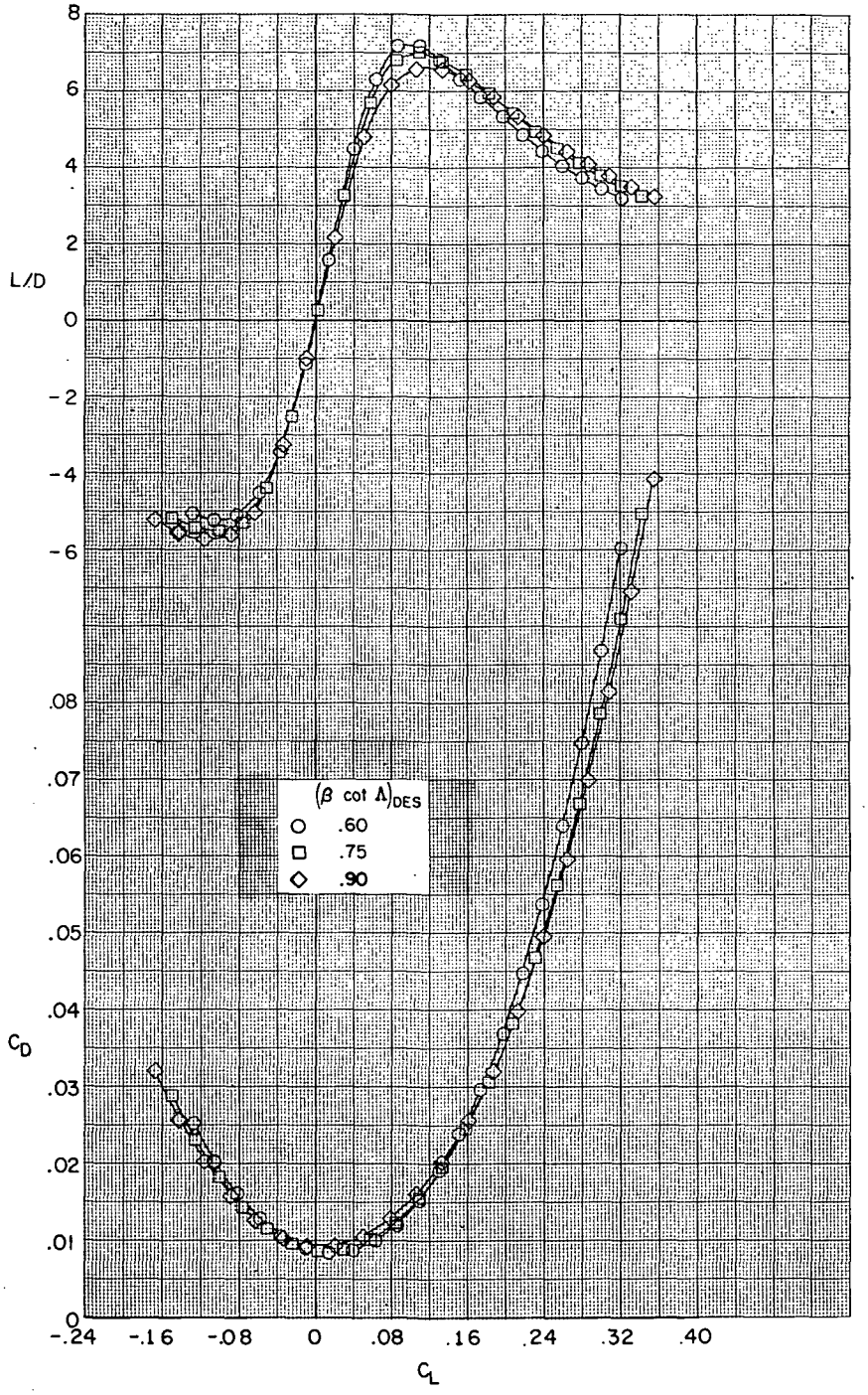

(b) Drag coefficient and lift-drag ratio as functions of lift coefficient.

Figure 11.- Concluded.

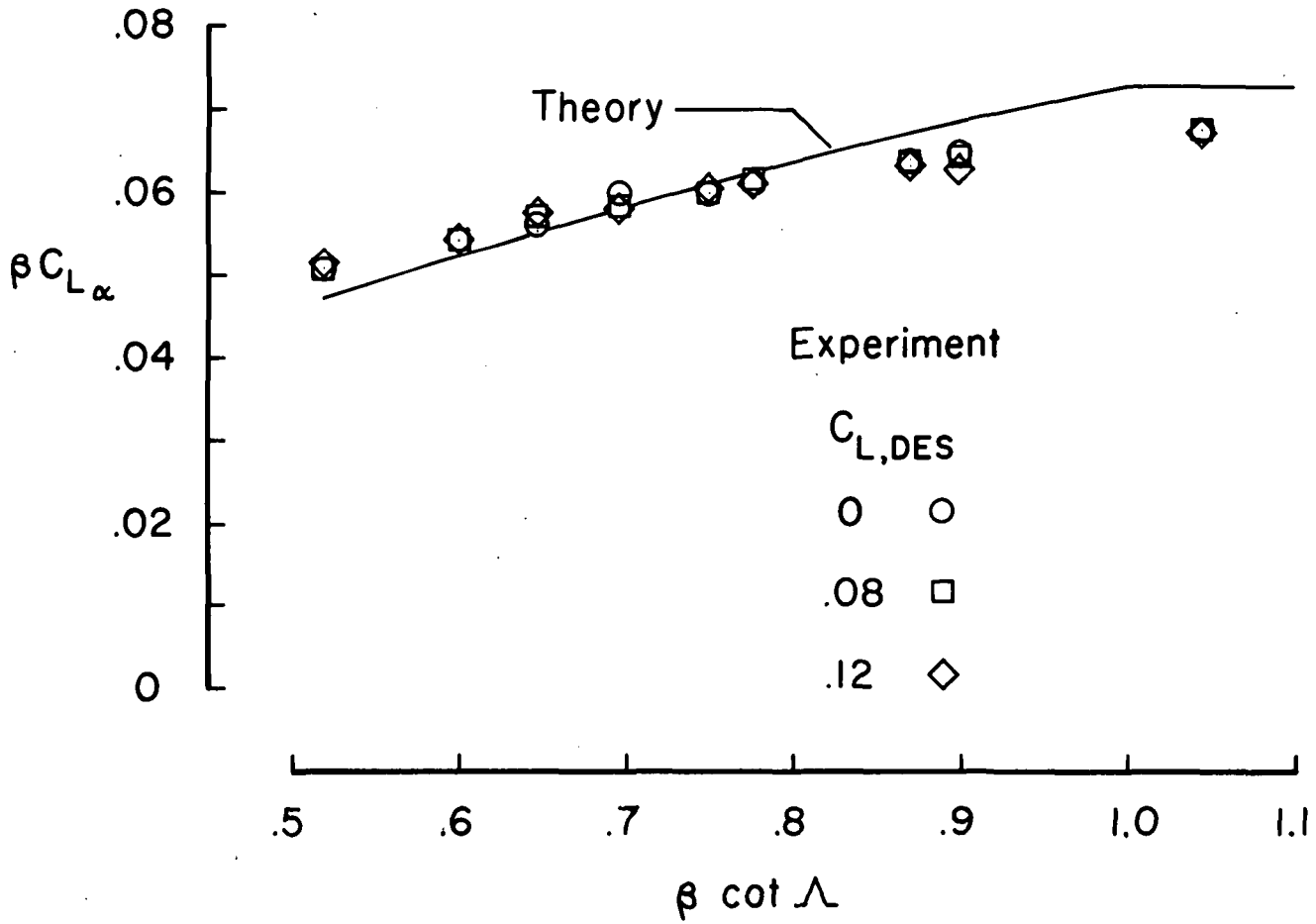

(a) Lift slope.

Figure 12.- Lift slope and longitudinal stability derivative of the test models.

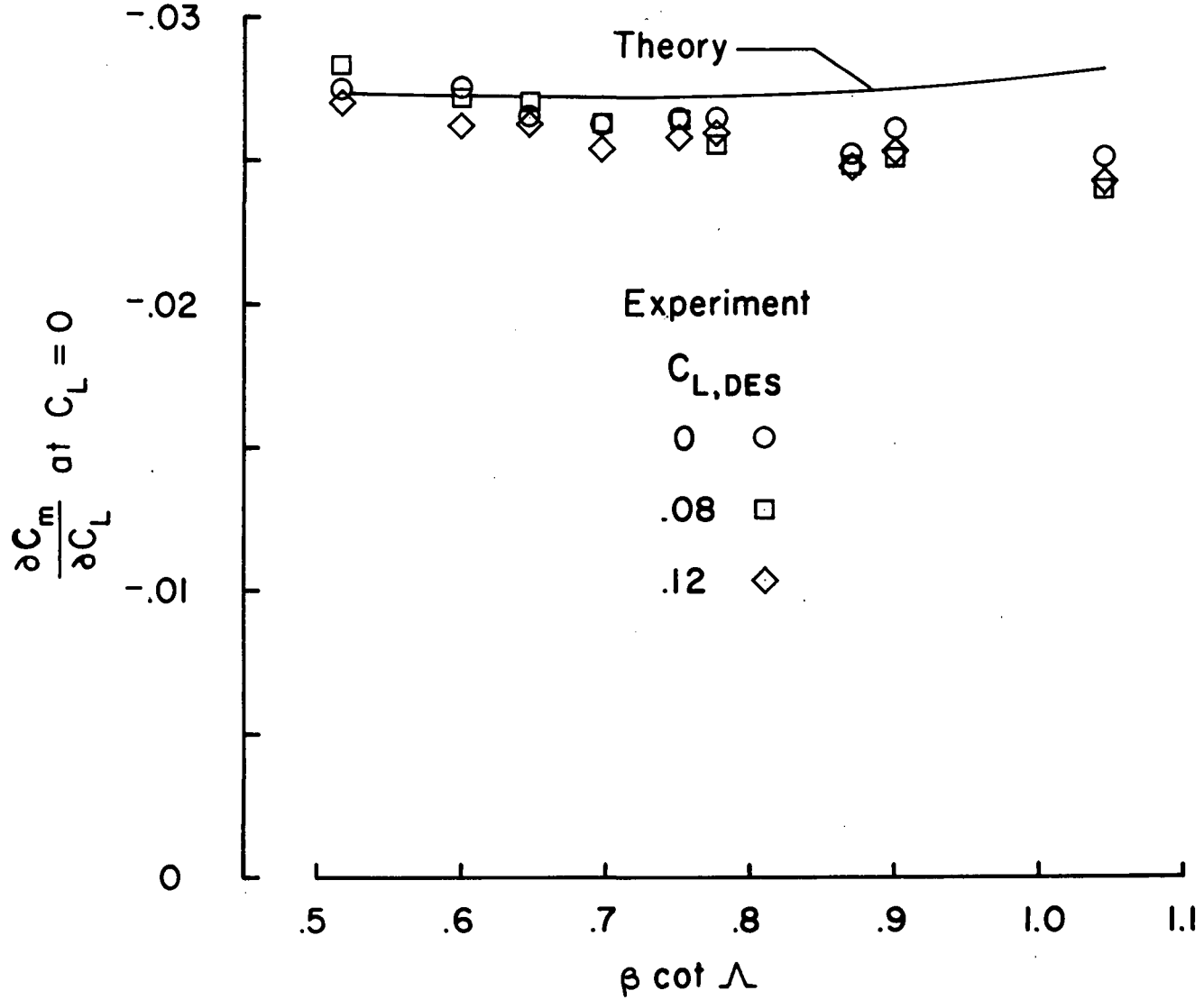

(b) Longitudinal stability derivative.

Figure 12.- Concluded.

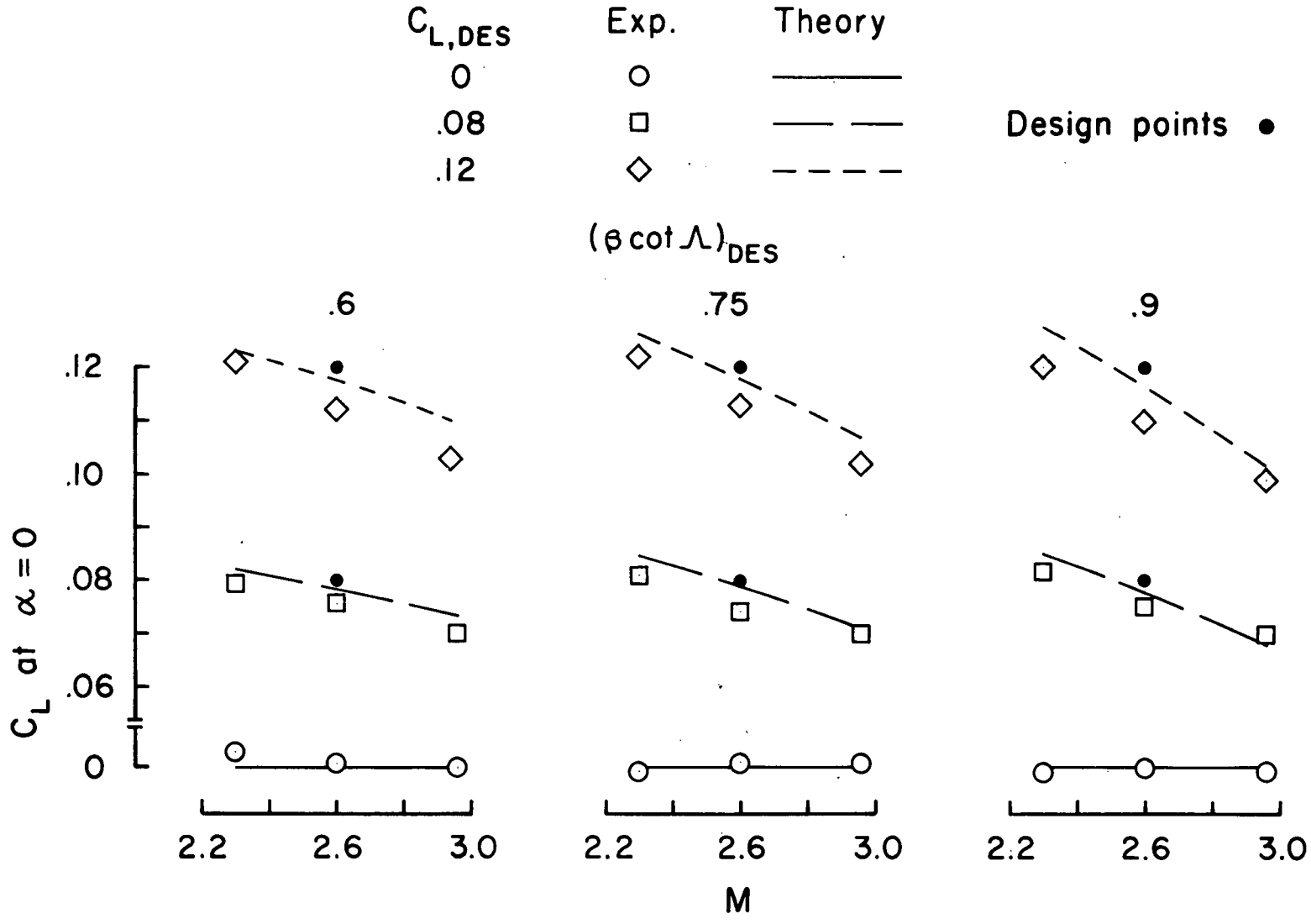

Figure 13.- Theoretical and experimental C_L at $\alpha = 0^o$.

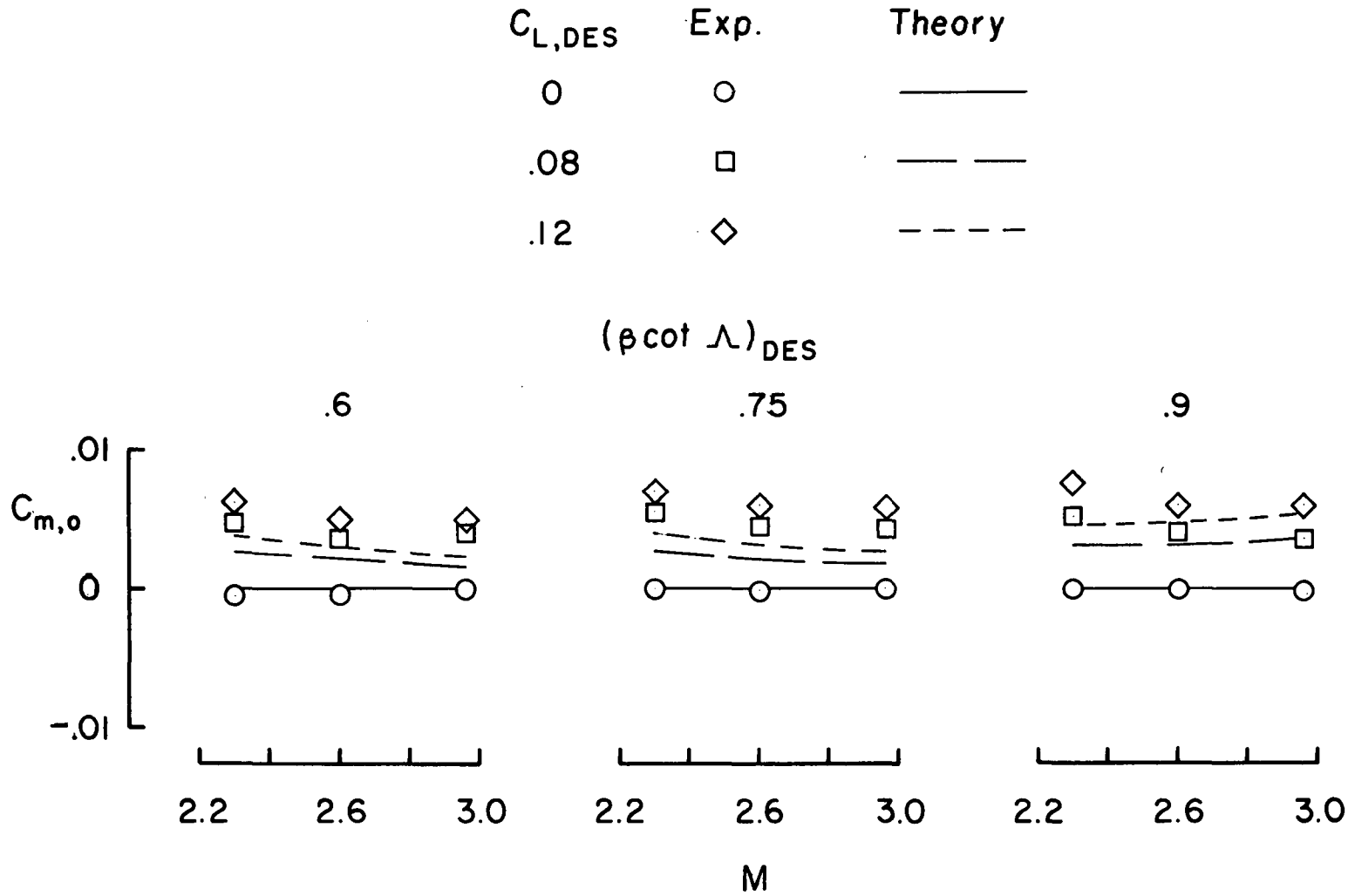

Figure 14.- Theoretical and experimental $C_{m,o}$.

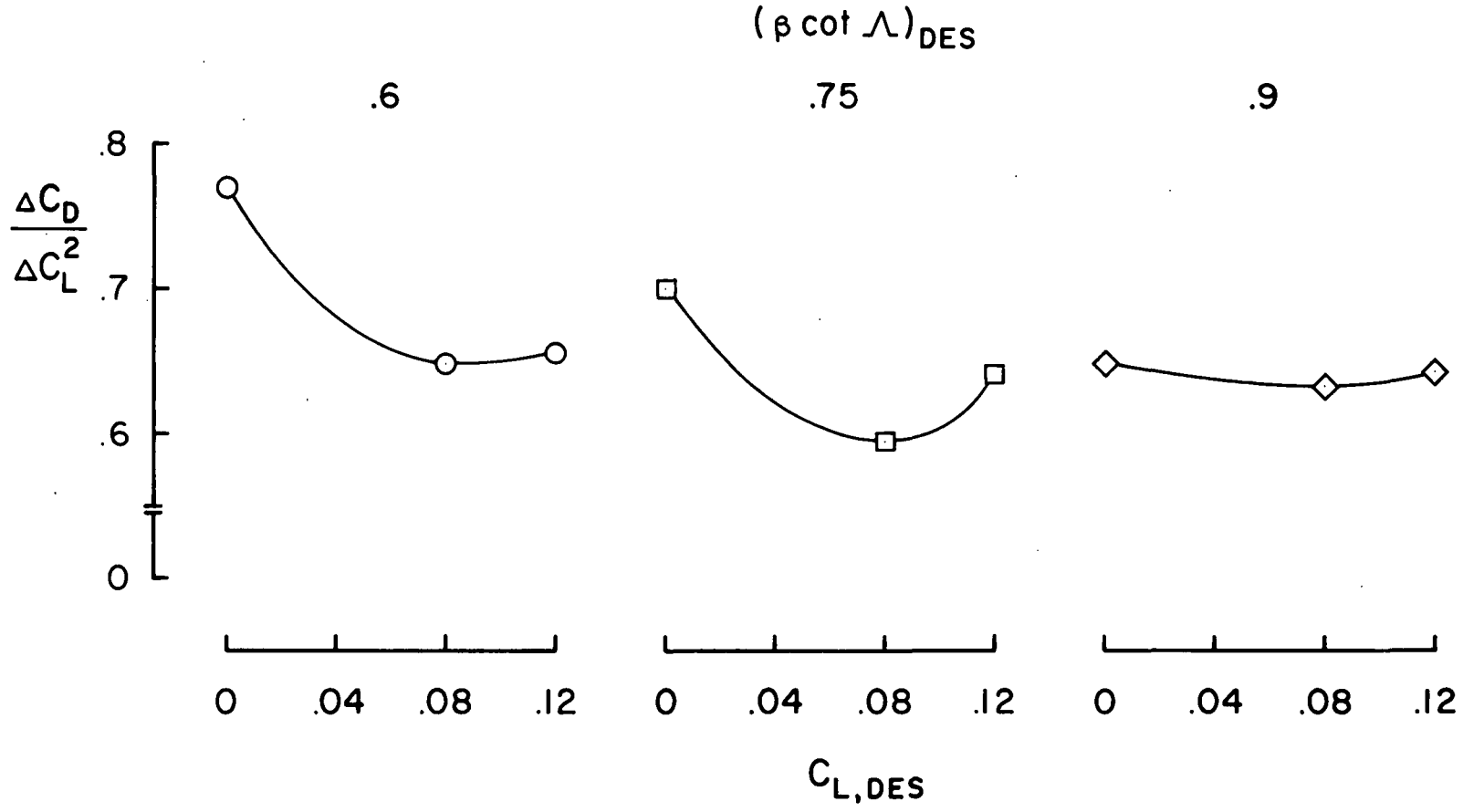

Figure 15.- Experimental drag due to lift at M = 2.6 and $C_{L,DES}$.

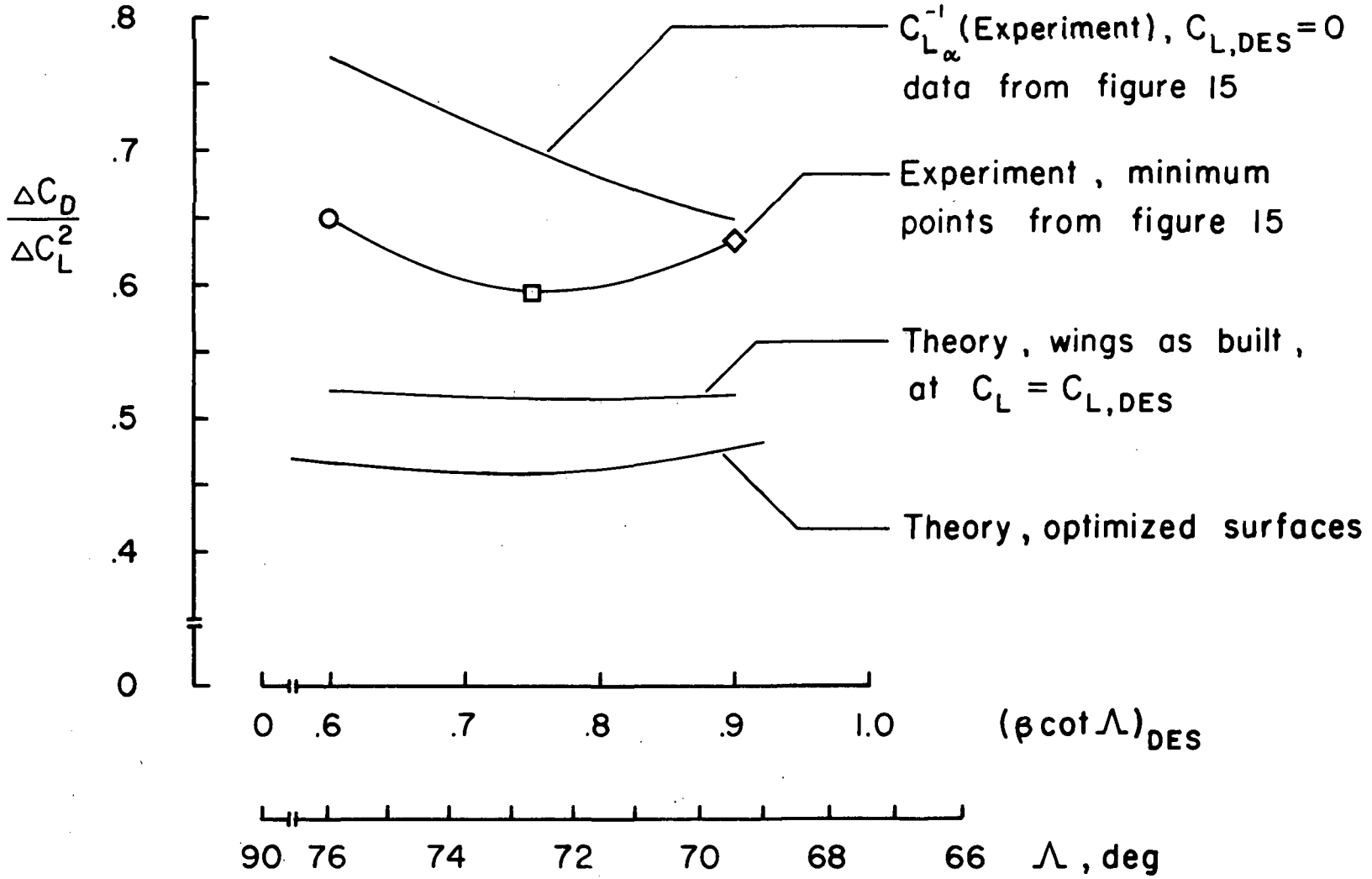

Figure 16.- Theoretical and experimental drag due to lift at M = 2.6.

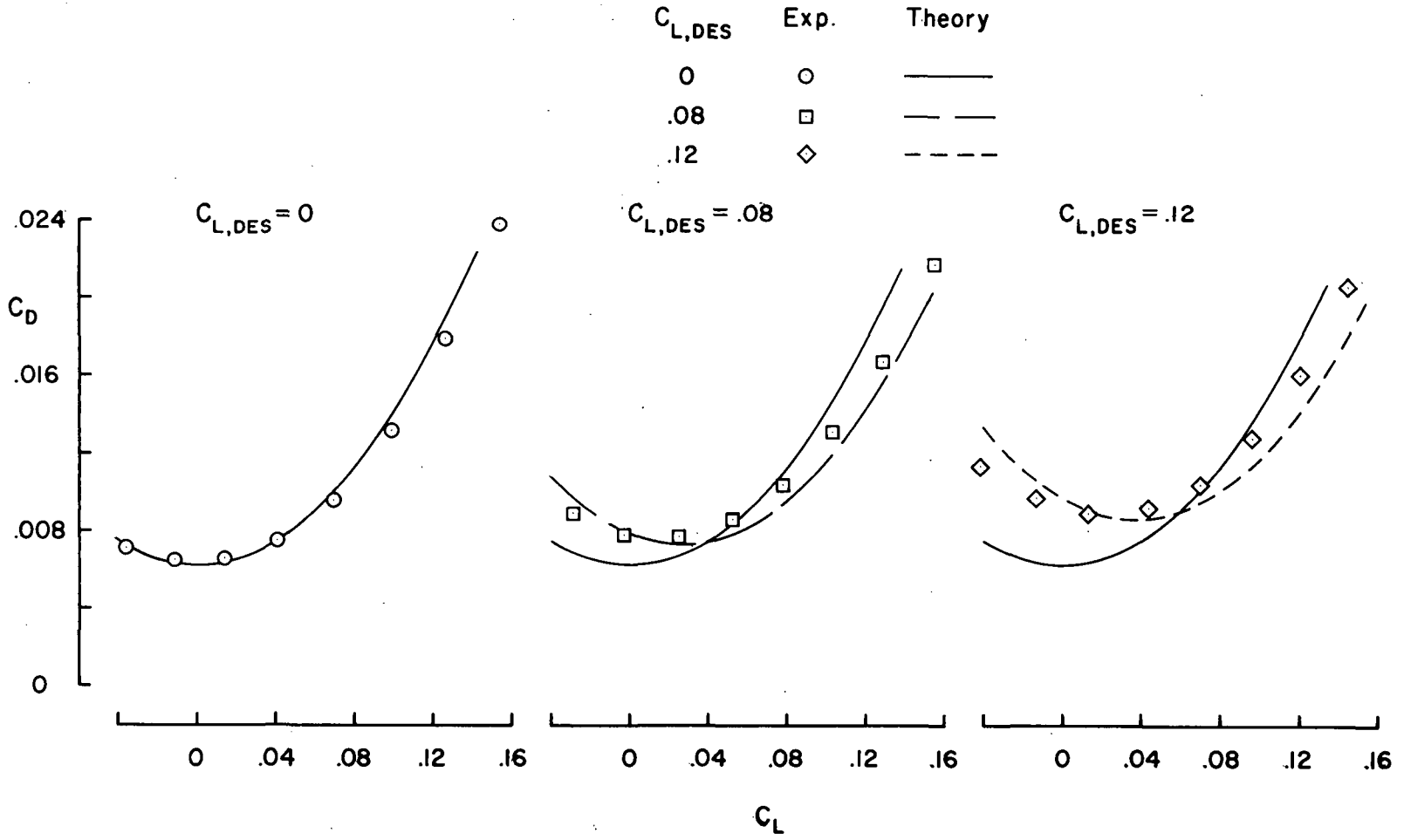

(a) $(\beta \cot \Lambda)_{DES} = 0.6$ wings.

Figure 17.- Theoretical and experimental drag polars at M = 2.6.

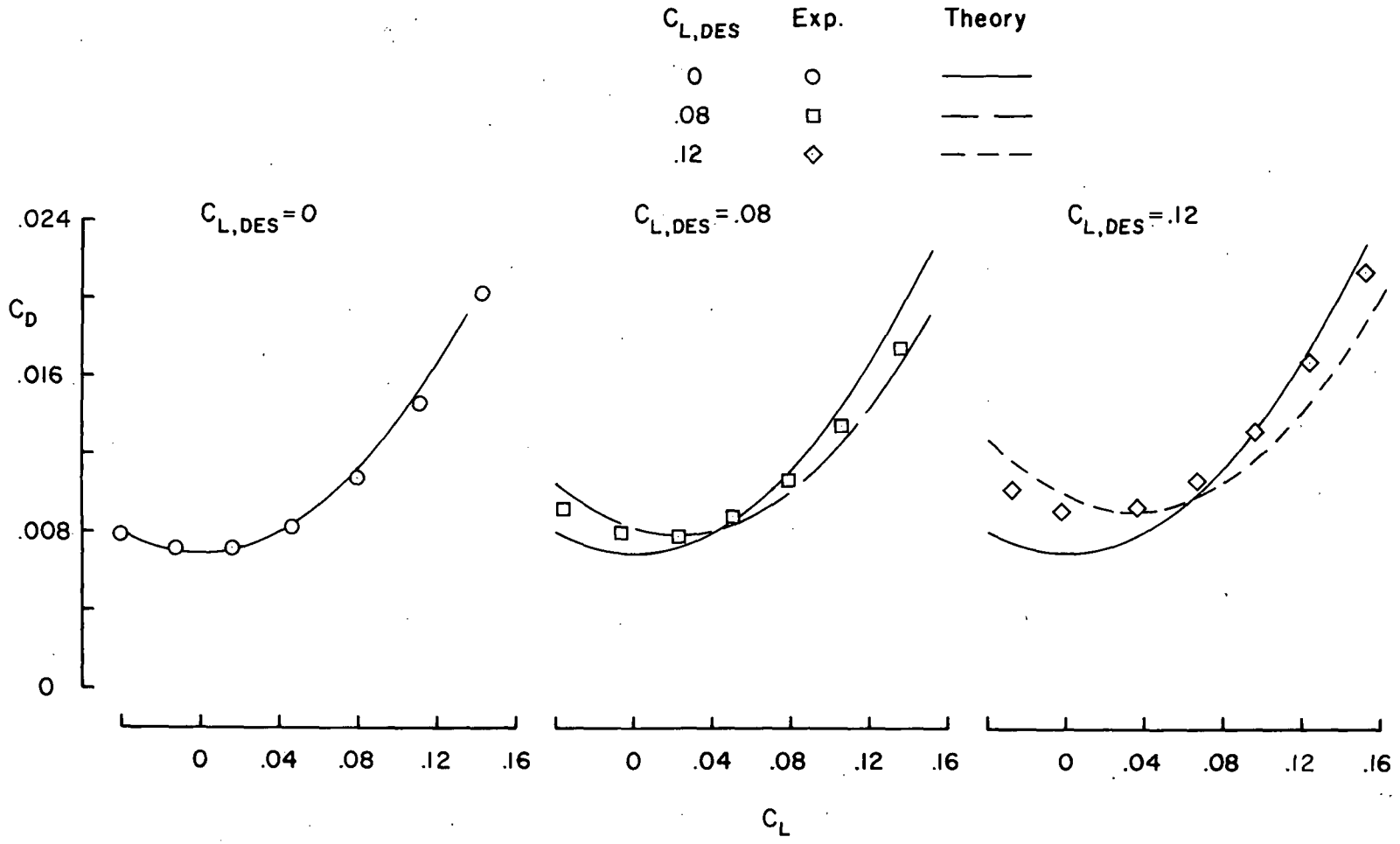

(b) $(\beta \cot \Lambda)_{DES} = 0.75$ wings.

Figure 17.- Continued.

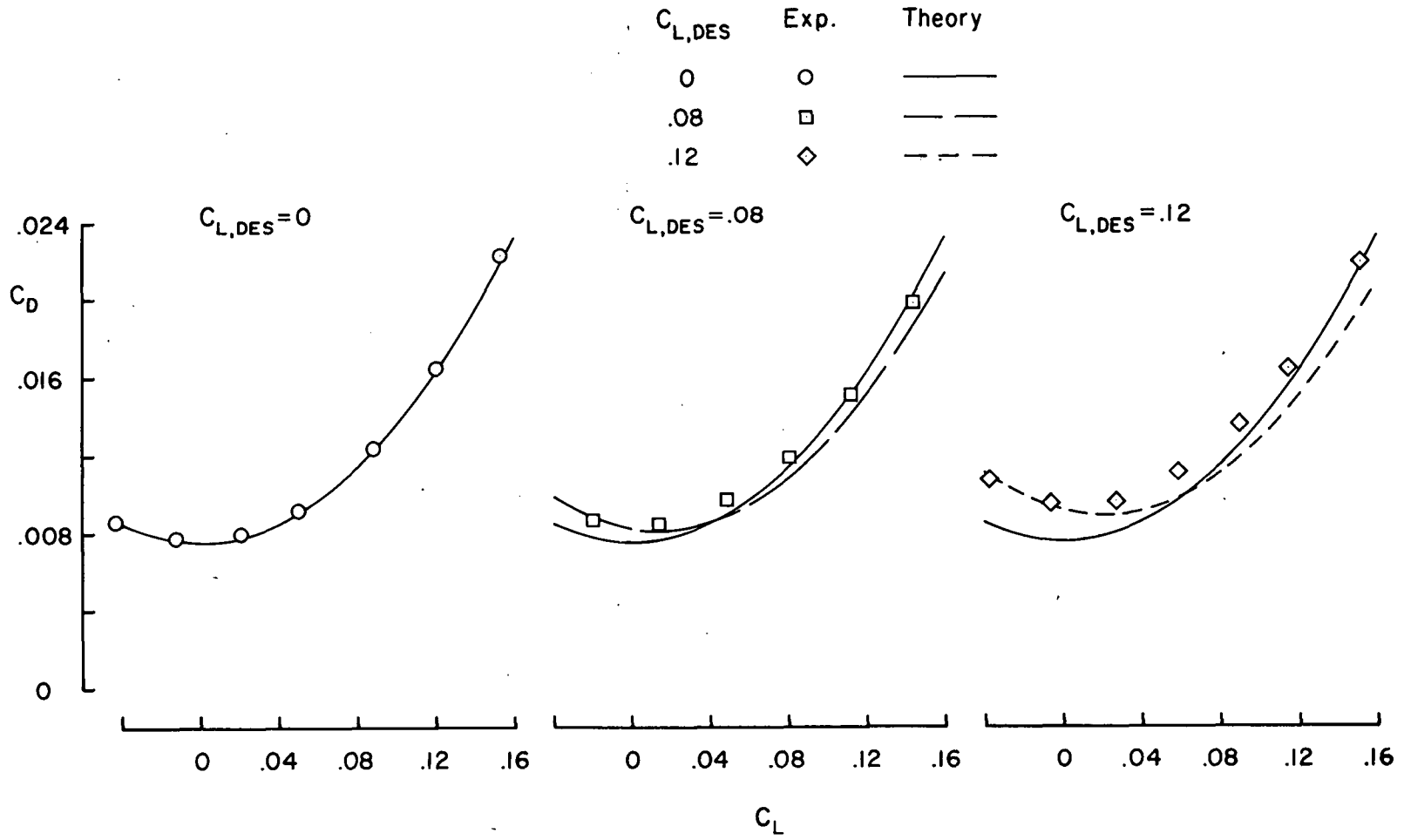

(c) $(\beta \cot \Lambda)_{DES} = 0.9$ wings.

Figure 17.- Concluded.

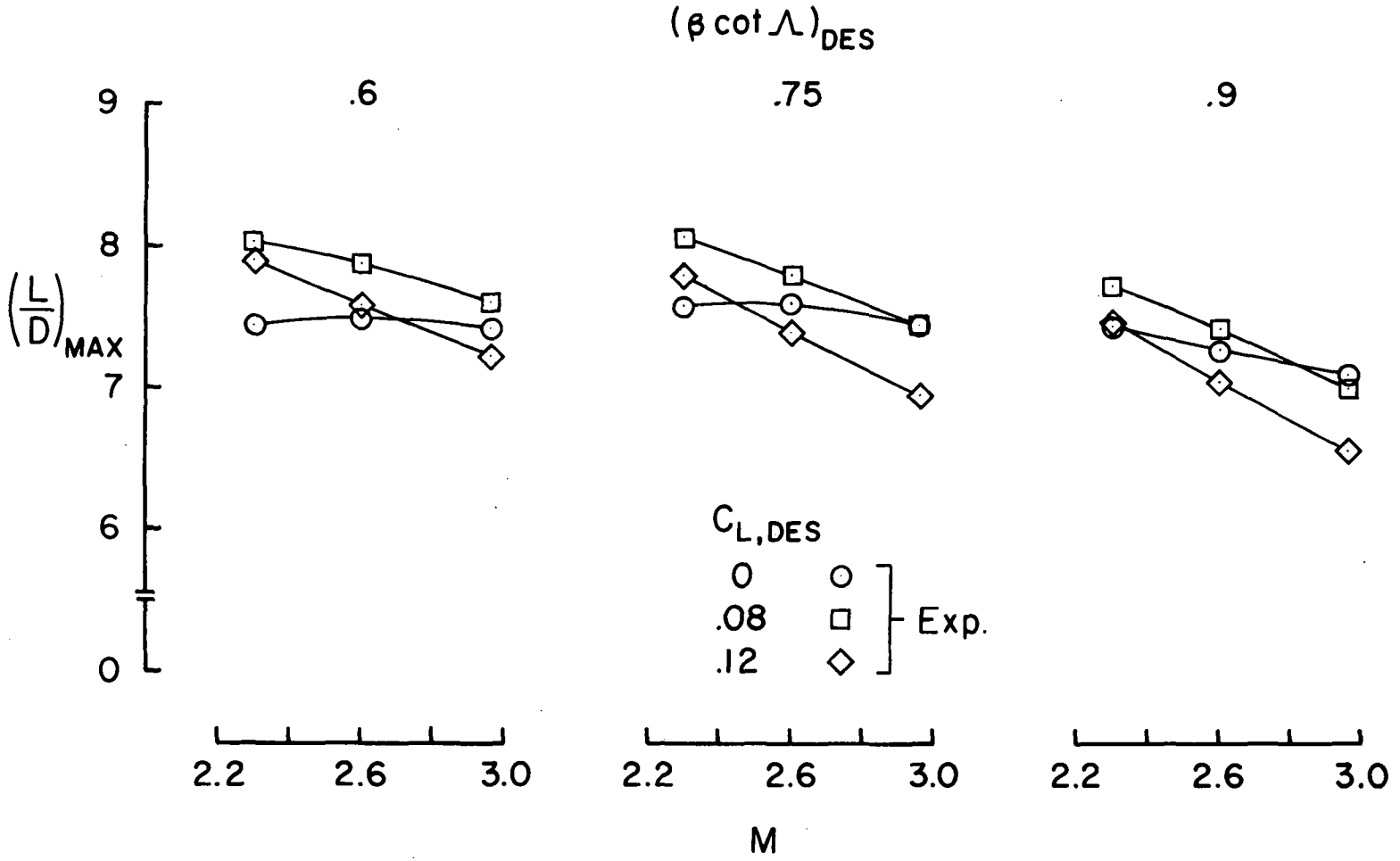

(a) $(L/D)_{MAX}$ as a function of Mach number.

Figure 18.- Maximum lift-drag performance over the Mach number, Mach-number—sweep-angle parameter, and design-lift-coefficient ranges.

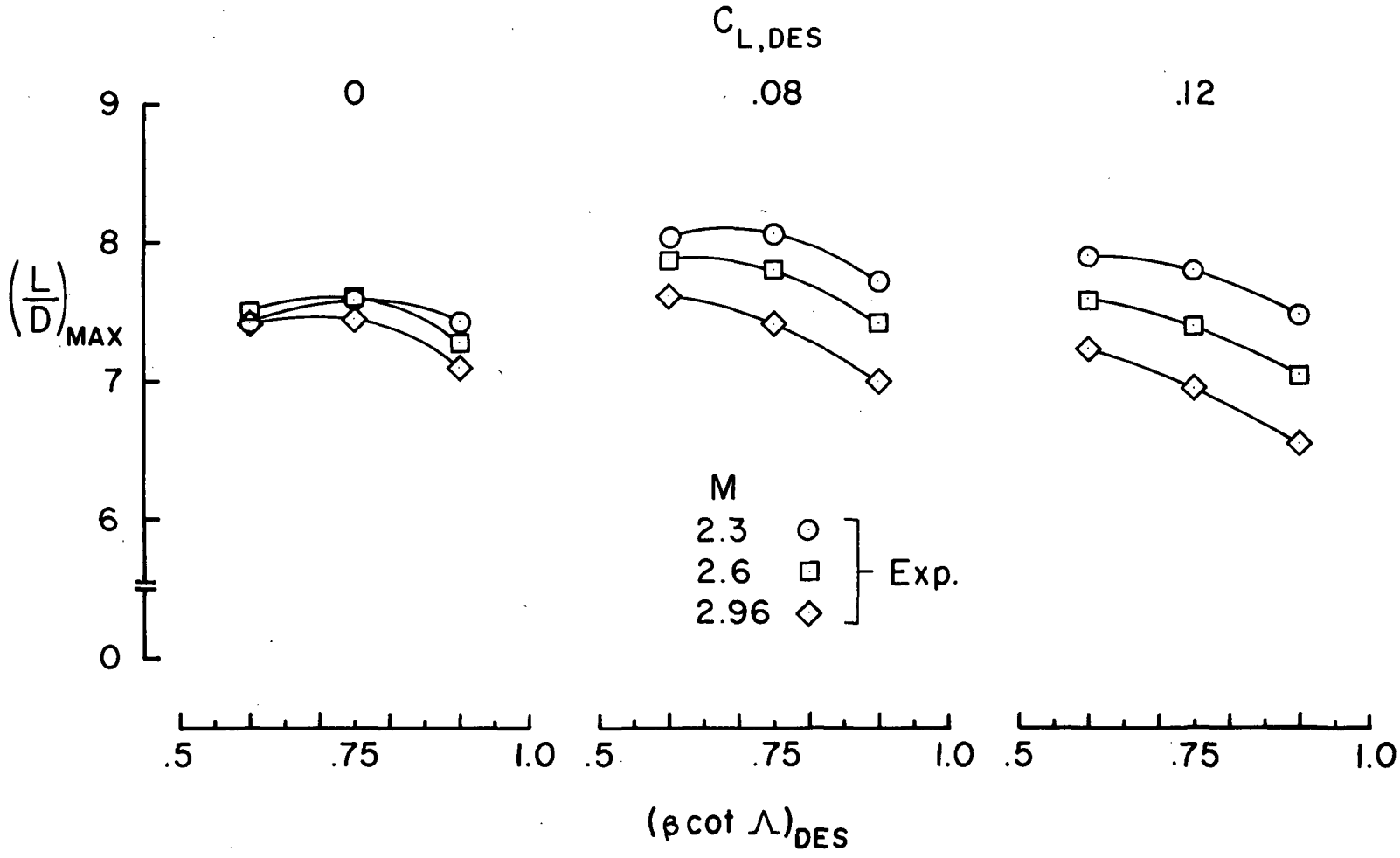

(b) $(L/D)_{MAX}$ as a function of Mach-number—sweep-angle parameter.

Figure 18.- Continued.

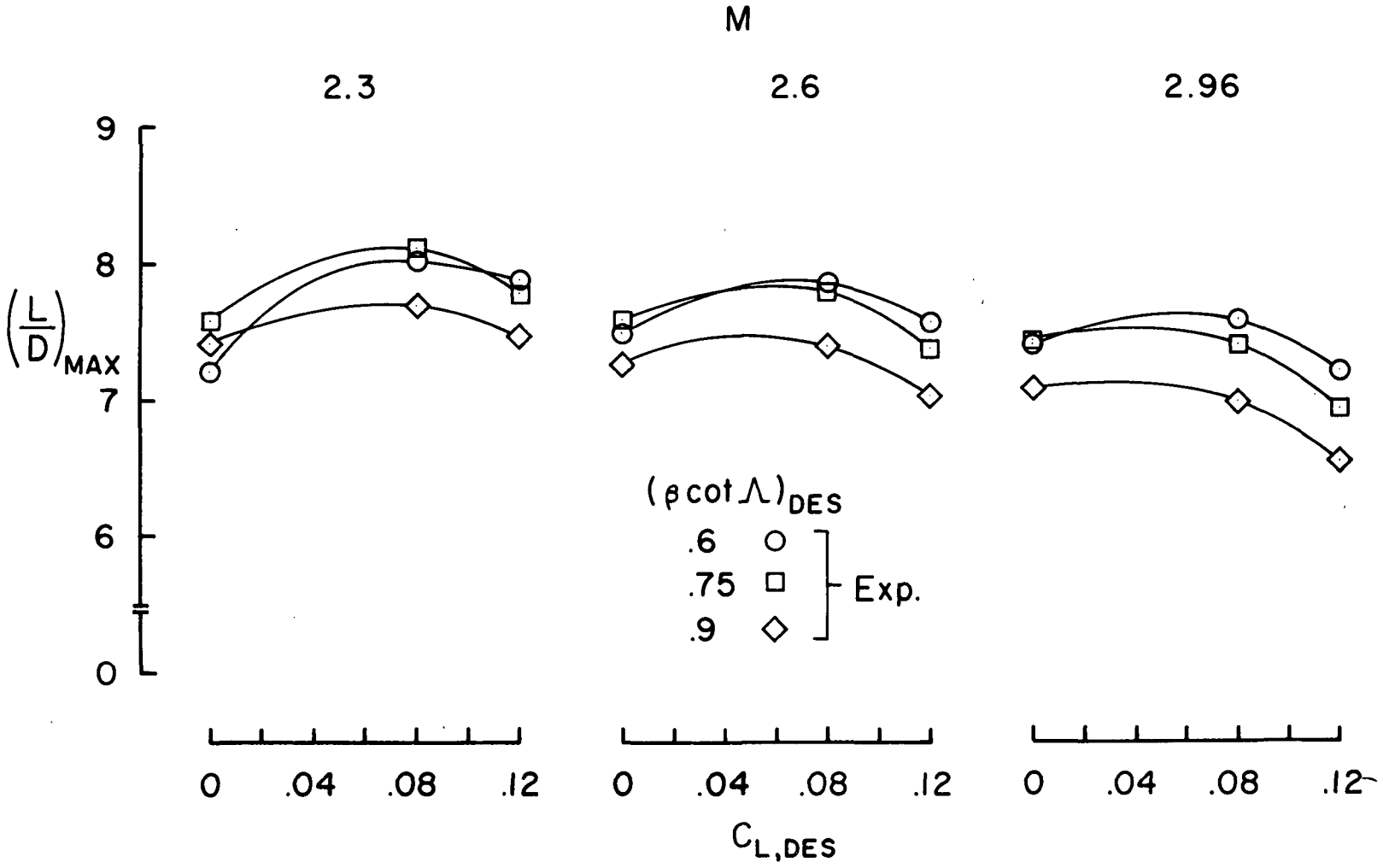

(c) $(L/D)_{MAX}$ as a function of design lift coefficient.

Figure 18.- Concluded.

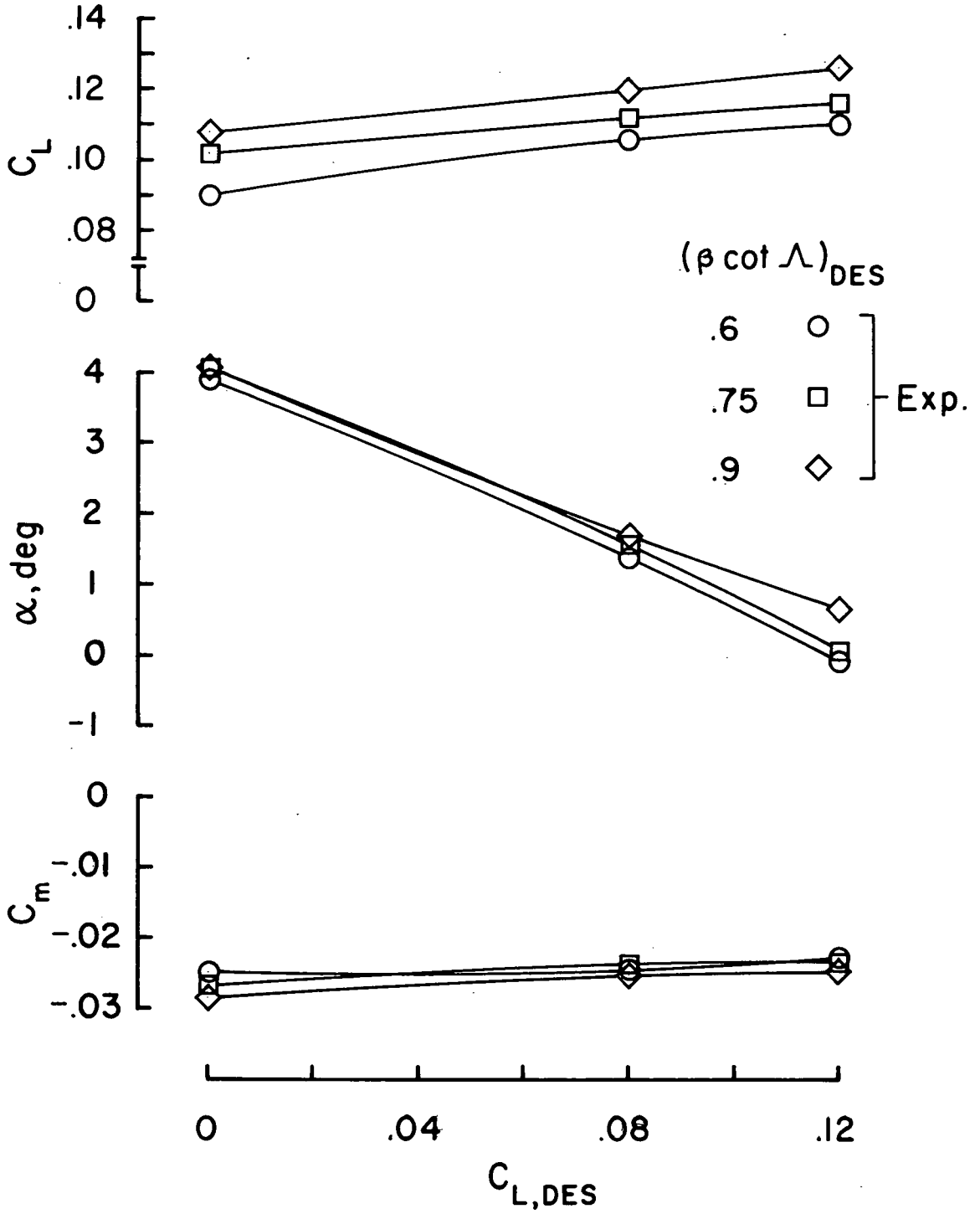

Figure 19.- Variation of C_L, α, and C_m with design lift coefficient at $(L/D)_{MAX}$ and M = 2.6.

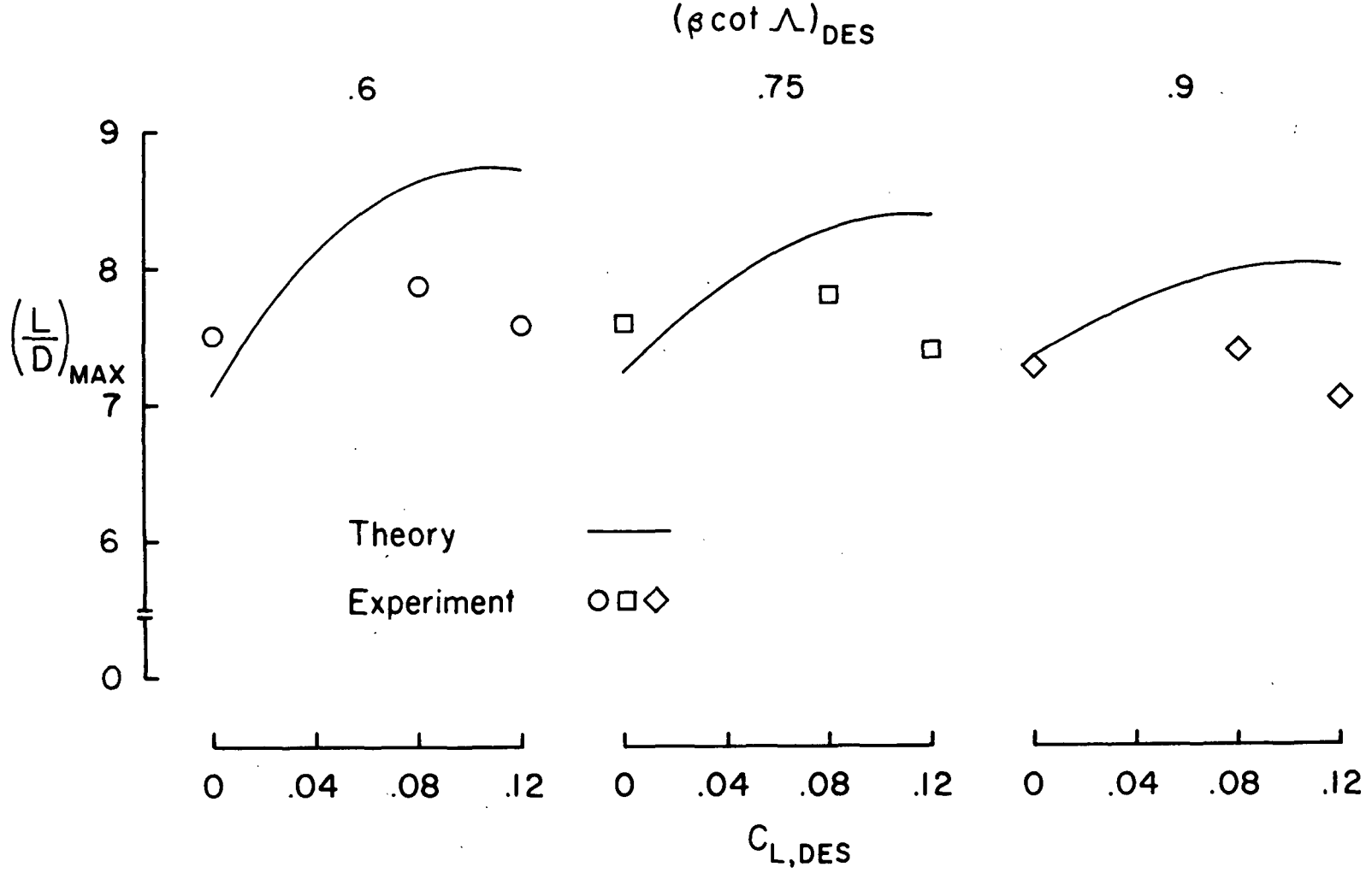

Figure 20.- Theoretical and experimental maximum lift-drag ratio at M = 2.6.

NATIONAL AERONAUTICS AND SPACE ADMINISTRATION
WASHINGTON, D.C. 20546

OFFICIAL BUSINESS
PENALTY FOR PRIVATE USE $300

SPECIAL FOURTH-CLASS RATE
BOOK

POSTAGE AND FEES PAID
NATIONAL AERONAUTICS AND
SPACE ADMINISTRATION
451

U.S.MAIL

995 001 C1 U 01 741122 S00120ES
PHILCO FORD CORP
AERONUTRONIC DIV
AEROSPACE & COMMUNICATIONS OPERATIONS
ATTN: TECHNICAL INFO SERVICES
FORD ROADS
92663

POSTMASTER: If Undeliverable (Section 158 Postal Manual) Do Not Return

"The aeronautical and space activities of the United States shall be conducted so as to contribute . . . to the expansion of human knowledge of phenomena in the atmosphere and space. The Administration shall provide for the widest practicable and appropriate dissemination of information concerning its activities and the results thereof."

—NATIONAL AERONAUTICS AND SPACE ACT OF 1958

NASA SCIENTIFIC AND TECHNICAL PUBLICATIONS

TECHNICAL REPORTS: Scientific and technical information considered important, complete, and a lasting contribution to existing knowledge.

TECHNICAL NOTES: Information less broad in scope but nevertheless of importance as a contribution to existing knowledge.

TECHNICAL MEMORANDUMS: Information receiving limited distribution because of preliminary data, security classification, or other reasons. Also includes conference proceedings with either limited or unlimited distribution.

CONTRACTOR REPORTS: Scientific and technical information generated under a NASA contract or grant and considered an important contribution to existing knowledge.

TECHNICAL TRANSLATIONS: Information published in a foreign language considered to merit NASA distribution in English.

SPECIAL PUBLICATIONS: Information derived from or of value to NASA activities. Publications include final reports of major projects, monographs, data compilations, handbooks, sourcebooks, and special bibliographies.

TECHNOLOGY UTILIZATION PUBLICATIONS: Information on technology used by NASA that may be of particular interest in commercial and other non-aerospace applications. Publications include Tech Briefs, Technology Utilization Reports and Technology Surveys.

Details on the availability of these publications may be obtained from:

SCIENTIFIC AND TECHNICAL INFORMATION OFFICE

NATIONAL AERONAUTICS AND SPACE ADMINISTRATION

Washington, D.C. 20546